Joint Trajectory-Resource Optimization in UAV-Enabled Edge-Cloud System With Virtualized Mobile Clone

Haibo Mei, Kun Yang, *Senior Member, IEEE*, Qiang Liu, *Member, IEEE*, and Kezhi Wang, *Member, IEEE*

***Abstract*—This article studies an unmanned aerial vehicle (UAV)-enabled edge-cloud system, where UAV acts as a mobile edge computing (MEC) server interplaying with remote central cloud to provide computation services to ground terminals (GTs). The UAV-enabled edge-cloud system implements a virtualized network function, namely, mobile clone (MC), for each GT to help execute their offloaded tasks. Through such network function virtualization (NFV) implemented on top of the UAV-enabled edge-cloud system, GTs can have extended computation capability and prolonged battery lifetime. We aim to jointly optimize the allocation of resource and the UAV trajectory in the 3-D spaces to minimize the overall energy consumption of the UAV. The proposed solution, therefore, can extend the endurance of the UAV and support reliable MC functions for GTs. This article solves the complicated optimization problem through a block coordinate descent algorithm in an iterative way. In each iteration, the allocation of resource is modeled as a multiple constrained optimization problem given predefined UAV trajectory, which can be reformulated into a more tractable convex form and solved by successive convex optimization and Lagrange duality. Second, given the allocated resource, the optimization of the trajectory of rotary-wing/fixed-wing UAV can be formulated into a series of convex quadratically constrained quadratically program (QCQP) problems and solved by the standard convex optimization techniques. After the block coordinate descent algorithm converges to a prescribed accuracy, a high-quality suboptimal solution can be found. According to the simulation, the numerical results verify the effectiveness of our proposed solution in contrast to the baseline solutions.**

***Index Terms*—Communication and computation resource allocation, energy consumption, mobile edge computing (MEC), unmanned aerial vehicle (UAV) 3-D-trajectory, UAV.**

Manuscript received September 5, 2019; revised October 13, 2019; accepted November 1, 2019. Date of publication November 11, 2019; date of current version July 10, 2020. This work was supported by the Natural Science Foundation of China under Grant 61620106011 and Grant 61572389. *(Corresponding author: Qiang Liu.)*

H. Mei is with the School of Aeronautics and Astronautics, University of Electronic Science and Technology of China, Chengdu 611731, China, and also with the School of Communication and Information Engineering, University of Electronic Science and Technology of China, Chengdu 611731, China (e-mail: haibo.mei@uestc.edu.cn).

K. Yang is with the School of Computer Sciences and Electrical Engineering, University of Essex, Colchester CO4 3SQ, U.K., and also with the School of Communication and Information Engineering, University of Electronic Science and Technology of China, Chengdu 611330, China (e-mail: kunyang@essex.ac.uk).

Q. Liu is with the School of Communication and Information Engineering, University of Electronic Science and Technology of China, Chengdu 611330, China (e-mail: liuqiang@uestc.edu.cn).

K. Wang is with the Department of Computer and Information Sciences, Northumbria University, Newcastle upon Tyne NE2 1XE, U.K. (e-mail: kezhi.wang@northumbria.ac.uk).

Digital Object Identifier 10.1109/JIOT.2019.2952677

I. Introduction

NOWADAYS with an increasing popularity, unmanned aerial vehicle (UAV) has been applied to handle varieties of tasks, such as combat, surveillance, media, rescue, etc. [1], [2]. Particularly, UAV can be employed as various aerial communication platforms to help realize ubiquitous wireless communications, due to its many advantages, such as the ability of on-demand and swift deployment, high flexibility with fully controllable mobility, and high probability of having line-of-sight (LoS) radio frequency links with the ground terminals (GTs) [3], [4]. The UAV-aided wireless communication thus has attracted intensive research interests. For example, UAV placement in 2-D/3-D dimensions (latitude, longitude, and height) [5]–[10] and UAV trajectory design with power saving [11]–[15] have been comprehensively studied to improve the quality-of-service (QoS) and extend the endurance of UAV working in the wireless networks. Most of those works tried to facilitate UAV working as the base station, access point, or relay, by deploying the UAV-aided wireless network with optimal UAV number, trajectory, and resource allocation strategies. However, those prior works [5]–[15] only considered the energy-efficient performance of UAV, while leaving the energy consumption of GTs unconsidered. In practice, wireless networks usually constitute a large number of terminals that are typically constrained by their computation capacity and power. UAV-aided wireless communications thus are in need of efficient techniques to improve the computation capacity and prolong the lifetime of GTs [16]. This motivates our current work to study UAV-enabled wireless communication with the mobile edge computing (MEC) technique [17].

In an MEC powered network, the MEC servers are mostly located at the edge of the network, and they can receive and execute the offloaded tasks from the user devices [18]–[20]. Under this deployment, MEC can help to extend the computation capacity and to prolong the battery lifetime of each user device, like in 4G/5G mobile networks [21], [22]. Further, MEC can interplay with the central cloud to work in a hybrid way [23]. In specific, an MEC server can be developed in the

proximity of GTs to locally handle users' time-sensitive tasks or the tasks not suitable to be offloaded to the central cloud. In the meantime, the central cloud can handle the intensive computations of the offloaded computing tasks from GTs that are not sensitive to task latency. To this end, through the interplaying of the edge-cloud, the hybrid MEC can balance the tradeoff and finish GTs' tasks with satisfaction.

Compared to the conventional edge-cloud architecture, UAV-enabled edge-cloud system in this article can provide flexible and on-demand MEC services by leveraging the high mobility of UAV. UAV-enabled MEC[1] can sequentially visit the GTs and receive offloaded tasks only when it moves sufficiently close to each GT, which can ensure high probability of LoS connectivity between UAV and GT and save the transmission energy of all GTs. In addition, the UAV-enabled MEC has fronthaul linked to a central cloud together to work interactively. In practice, in the UAV-enabled edge-cloud system, it can follow a concept of network function virtualization (NFV) to implement mobile clone (MC) function for each GT on top of the edge-cloud architecture. Basically, the UAV-enabled MEC and central cloud will cooperatively realize effective MC function for each GT via a clone sharing technique. Clone sharing increases the opportunity of the clone optimum utilization for different GTs, which can integrate both the advantages of the central cloud and the UAV-enabled MEC. As a result, the task offloading will be facilitated given such MC deployment.

UAV-enabled edge-cloud system can be applied to many tasks and has gradually attracted lots of interests. In [24], it proposed a UAV-based IoT platform for a crowd surveillance use case, where MEC is discussed to help task offloading for IoT devices. Jeong *et al.* [25] discussed the optimal bit allocation in MEC and UAV-aided wireless network, considering energy cost. Du *et al.* [16] discussed UAV working with MEC to collect IoT devices data and give instructions to those devices. In [26], task offloading was considered in the scenario where UAV works as the cellular user to help offloading GT tasks to the base station. Recently, the authors of [27]–[30] have studied resource allocation, trajectory design, user association, and dynamic task offloading to improved the performance of UAV working with MEC. Due to the advantages, it is expected that, as the upcoming of 5G and smart city era, more and more applications with UAV-enabled edge-cloud system will appear in a short time.

Despite the advantages, the UAV-enabled MEC however has limited communication/computation abilities because of its constrained onboard power. The constrained power will dramatically short the mission time of the UAV, which is the prime issue that hinders the wide applications of such technology [4]. In practice, UAV has limited power to support its flight propulsion. Also, the UAV has limited transmission power to support the data transmission to the GTs. This issue will escalate when MEC working with the UAV, as the MEC server will carry out intense computations and consume extra power of the UAV. It has been studied that the power constraint of UAV can be released in the more general cases with multiple cooperative UAVs and/or in the presence of ground BSs, like the work in [26] and [31]. However, the more general case is highly nontrivial and involves the additional considerations, such as UAV collision avoidance, spectrum sharing between UAVs and BSs, possibly inter-UAV communications, and complicity of computation offloading strategies. The work [24]–[30] tried to release the energy constraint of UAV, but authors did not consider the joint 3-D trajectory-resource optimization to maximally save the energy consumption. Based on our best knowledge, there is no work proposed to particularly handle the power constraint issue of UAV-enabled MEC.

To handle this issue, in this article, we aim to optimize the resource allocations and the 3-D trajectory of rotary/fixed-wing UAV to minimize its overall energy consumption in the UAV-enabled edge-cloud system. The optimization also guarantees the MC can satisfy the basic service requirement of each GT task on latency. Due to the existing issues of multiple UAVs as mentioned in [26] and [31], we only consider a single UAV and leave the multiple UAVs for future work. Specifically, we propose a joint trajectory-resource optimization to: 1) allocate the OFDM-based bandwidth with configurable transmit power to satisfy the data transmission requirement of the tasks from GT to its MC; 2) allocate the computation capacities from UAV-enabled MEC and central cloud to the MC of each GT to satisfy the computing requirements; 3) minimize the energy consumption of the UAV on running the MC while interplaying with the central cloud; and 4) minimize energy consumption on UAV propulsion. According to the study, it is an NP-hard problem to find the optimal solution to satisfy all those requirements, while considering the different energy models of fixed-wing and rotary-wing UAVs.

In the NP-hard problem, some methods, e.g., heuristic [32] and game theory [33], have been proposed to solve similar problems, like the resource allocation in a heterogeneous network [34], [35] and the dynamic task offloading in hybrid MEC [36]. However, those methods may not be able to find the optimal solution to the problem and have high computing complexity. In comparison, convex optimization [37] is a superior method to solve any problem that is in convex form. Convex optimization has the merit of low computation complexity, and it guarantees to reach the optimization of the targeted problem. Also there are a number of existing methods, like the interior-point method [38] and the subgradient method [39], and tools, like CVX [40], available to help solve the convex problem. In [27]–[30], the convex optimization technique, like success convex optimization (SCO), has been applied to solve the optimization problems on UAV working with MEC.

In this article, we try to apply the convex optimization technique to solve the mentioned optimization problem. However, the difficulty is to convert the NP-hard problem of UAV-enabled MEC into a series of subproblems in convex form. To handle the difficulty, we optimize the resource allocation and UAV trajectory iteratively through a block coordinate descent algorithm to reach a suboptimal solution. In each iteration, we first model the allocation of the communication and computation resources, including bandwidth, transmit power, and computation capacities in UAV-enabled MEC and central cloud, as a multiple constrained optimization problem

[1]In the rest of this article, we mention UAV and UAV-enabled MEC alternatively, and they are with the same meaning.

given predefined UAV trajectory. The multiple constrained problem can be reformulated into a more tractable convex form and solved by the SCO and Lagrange duality. Second, with obtained resource allocations in the previous step, we formulate the optimization of UAV trajectory as a series of convex quadratically constrained quadratically program (QCQP) problems with respect to horizontal trajectory, vertical trajectory, and fight time of the rotary-wing/fixed-wing UAV, respectively, which can be solved by the standard convex optimization techniques. In practice, the block coordinate descent algorithm can converge to a suboptimal solution after reaching a prescribed accuracy. Through simulation, the numerical results demonstrate the effectiveness of our proposed solution as compared to the baseline solution. Generally, the primary contributions of this article are as follows.

1) It is innovative to improve the energy-efficient performance of the UAV-enabled MEC in the UAV-enabled edge-cloud system. We intensively study how the task offloading from GT to MC being jointly affected by the allocations of communication and computation resources and the trajectory of rotary-wing/fixed-wing UAV. Then we conclude that it is a multiple constrained and NP-hard problem to optimize the UAV to work energy efficiently. Based on our best knowledge, this problem has not been comprehensively studied yet.
2) It is innovative to optimize the 3-D trajectory of rotary-wing/fixed-wing UAV working with MEC. Most of the previous works only consider 2-D UAV trajectory, which is impractical. In reality, it is complicated to jointly optimize the UAV trajectories both in the vertical and horizontal dimensions, and the trajectory design is additionally constrained by the limited communication and computation capabilities of the UAV, when UAV working as an MEC server and interplaying with the central cloud. According to our study, it is the first work to design such 3-D trajectory of the UAV while working with MEC.

The remainder of this article is organized as follows. In Section II, we describe the system model and formulate the problem. In Section III, we present the solution to the optimization problem. In Section IV, simulation results and analysis are presented. In Section V, we give the conclusions and future work.

II. System Model and Problem Formulation

A. System Model

To facilitate the analysis, this article considers a typical scenario of UAV-enabled edge-cloud system, which is shown in Fig. 1. In the scenario, one UAV is dispatched to serve a group of GTs. The UAV-enabled MEC and central cloud each deploy an MC for one GT, respectively, which is a virtual machine (VM). Under this deployment, the clone sharing technique [41] is further adopted by the UAV-enabled MEC and central cloud to cooperatively handle the offloaded task from a GT by sharing the data and service between the two MCs of the GT. In practice, it is not too hard to migrate data

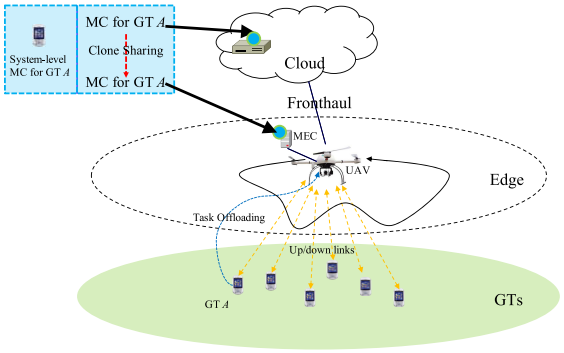

Fig. 1. Working scenario of the UAV-enabled edge-cloud system.

and service between the MCs in UAV-enabled MEC and central cloud. A live VM migration technique, as a rather popular technology, gives a firm protection to this kind of migration. To this end, the UAV-enabled edge-cloud system as a whole can offer a concept of system-level MC to each GT, and execute mobile applications on behalf of the GT [42]. For a task, its owing GT only has to upload the input data through the uplink to its associated system-level MC, then the two MCs of the GT in the UAV-enabled MEC and central cloud can interplay to jointly execute the offloaded task. After the execution, the results will be sent back to the GT via downlink. For simplicity, in the rest of this article, we mention MC with the same meaning as system-level MC.

To fascinate the interplay of UAV-enabled MEC and central cloud, assume the fronthaul from the UAV to the central cloud is an ultralow-latency connection supported by techniques like 5G networking, i.e., the UAV works as a 5G cellular user [26]. Thus, the transmission latency in the fronthual can be ignored during task offloading. It is assumed that there are $\mathcal{I} = \{1, 2, \ldots, I\}$ GTs on the ground, each of which has averagely expected task $U_i = (F_i, D_i, T_i)$ during UAV's mission completion time. For the task U_i, F_i describes the total number of the CPU cycles to be executed. D_i denotes the amount of output data to be transferred through the downlink from UAV to GT during the task offloading. T_i is the maximal allowed latency, within which U_i should be finished. In this article, we ignore the transmission of input data of U_i from GT to UAV in uplink. This is because the data transmission in uplink will barely consume the energy of the UAV-enabled MEC, and the energy consumed by the GT for uplink is trivial in practical IoT systems [16]. One GT task thus composes a communication job and a computation job. We assume the expected amount of each GT task during UAV's mission completion time can be efficiently found numerically or predicted by, e.g., machine learning [43]. The horizontal coordinate of each GT is formulated at $w_i = [x_i, y_i]^T \in \mathbb{R}^{2\times 1}, i \in \mathcal{I}$, which could be available and determined by the standard positioning techniques such as the GPS-based localization. In most IoT systems, one GT is normally static or in low mobility, and GTs in high mobility will not happen in practical UAV-enabled edge-cloud system. Thus, GTs are assumed to be static within the finite UAV mission time in this article, which is realistic.

To model UAV trajectory, we discretize the UAV path into M line segments, which are represented by $M+1$ waypoints in the 3-D coordinates: $\{h_m, q_m\}_{m=1}^{M+1}$. For the mth waypoint, h_m is the height and $q_m = \{x_m, y_m\}$ is the horizontal coordinate of the UAV. Assume $\{h_1, q_1\} = \{h_{M+1}, q_{M+1}\}$ to denote the UAV flying back to its initial location, which is the most common case. Also $h_{\max} \geq h_m \geq h_{\min}$, and $h_{\max}$ and $h_{\min}$ are the maximum and minimum heights, respectively, to ensure the UAV fly in safety. We impose the following constraints: $\|q_{m+1} - q_m\| \leq \Delta_{\max}^h$, $\|h_{m+1} - h_m\| \leq \Delta_{\max}^v$, $m = 1, \ldots, M$, where $\Delta_{\max}^h$ and $\Delta_{\max}^v$ are appropriately chosen values so that within each line segment, the UAV is assumed to fly with constant horizontal and vertical velocities and the distance between the UAV and each GT is approximately unchanged. Assume the task offloading will not take place in the stages of UAV taking off and landing, which is in a relatively short period. Thus, the UAV trajectory in the stages of UAV taking off and landing will not be considered in the system model. Then, with such path discretization, the UAV trajectory can be represented by the $M+1$ waypoints $\{h_m, q_m\}_{m=1}^{M+1}$ together with the duration $\{t_m\}_{m=1}^{M}$ representing the time that the UAV spends within each line segment. Let t_m denote the duration that the UAV remains in the mth line segment. The horizontal flying velocity of the UAV along the mth line segment is thus given by $v_m^h = [(\sqrt{\|q_{m+1} - q_m\|^2})/t_m] \leq V_{\max}^h, m = 1, \ldots, M$, where $V_{\max}^h$ is the maximum horizontal velocity of the UAV. In reality, the fixed-wing UAV is constrained to have a minimum horizontal velocity $v_m^h \geq V_{\min}^h > 0, m = 1, \ldots, M$ as it cannot hover statically at a fixed location and needs to move forward to remain aloft in contrast to the rotary-wing UAV. The vertical flying velocity of the UAV along the mth line segment is given by $0 \leq v_m^v = [(\sqrt{\|h_{m+1} - h_m\|^2})/t_m] \leq V_{\max}^v, m = 1, \ldots, M$, where $V_{\max}^v$ is the maximum vertical velocity of the UAV. If $v_m^v = 0$, the UAV adopts a steady straight-and-level (SLF) flight in the mth line segment. Furthermore, the total mission completion time is given by $\sum_{m=1}^{M} t_m \leq T_{\max}$, where $T_{\max}$ is the maximum allowed UAV mission time. M is chosen to be sufficiently large so that $M\sqrt{(\Delta_{\max}^h)^2 + (\Delta_{\max}^v)^2} \geq \widehat{D}$, where $\widehat{D}$ is a lower bound of the required total UAV flying distance.

1) Communication Model: In UAV-enabled system, we consider the effect of the environment on the occurrence of LoS, and an air-to-ground channel model in urban environments [15], [44]. The LoS probability is given as

$$p_{im}^{\text{los}} = \frac{1}{1 + a\exp\left(-b\left(\arctan\left(\frac{h_m}{d_{im}}\right) - a\right)\right)} \tag{1}$$

where a and b are constant values that depend on the environment. In this setting, the altitude and antenna heights of the GT are neglected. Specifically, the probability of having LoS for GT i depends on the altitude of the UAV h_m and the horizontal distance between the UAV and GT k denoted as $d_{im} = \sqrt{\|q_m - w_i\|^2}$. In other words, the pathloss of the air-to-ground link depends on the altitude in the vertical dimension, and the distance in the horizontal dimension. Then, the pathloss expression becomes

$$l_{im} = 20\log\left(\sqrt{h_m^2 + d_{im}^2}\right) + Ap_{im}^{\text{los}} + C \tag{2}$$

where A and C are constants such that $A = \eta_{\text{LoS}} - \eta_{\text{NLoS}}$ and $C = 20\log[(4\pi f_c)/c] + \eta_{\text{NLoS}}$; f_c is the carrier frequency (in Hertz); c is the speed of light (in meters per second); and η_{LoS} and η_{NLoS} (in decibels) are, respectively, the losses corresponding to the LoS and non-LoS connections depending on the environment. Following the pathloss model between UAV and GT, the instantaneous achievable rate of the ith GT's downlink in UAV path line m, denoted by $r_i[m]$ in bits per second (b/s), can be expressed as

$$r_i[m] = \alpha_i[m]B\log_2\left(1 + \frac{p_i[m]10^{\frac{-l_{im}}{10}}}{\alpha_i[m]BN_0}\right) \tag{3}$$

where N_0 denoting the power spectral density of the additive white Gaussian noise (AWGN) at the receivers; and $p_i[m]$ is the transmit power allocated by the UAV to transmit data to the ith GT through downlink in path line m. It has $\sum_{i=1}^{I} p_i[m] \leq P_{\max}$, where $P_{\max}$ is the maximum allowed transmit power of the UAV in path line m. Denote the total available system bandwidth by B in Hertz (Hz), the fraction of bandwidth assigned to the ith GT in path line m is denoted by $\alpha_i[m]$. In a practical OFDM system, $\alpha_i[m]$ is in general a discrete value between 0 and 1, which increases linearly with the number of subcarriers assigned to the ith GT in path line m. It is known that when the number of subcarriers is sufficiently large, $\alpha_i[m]$ can be approximated to a continuous value between 0 and 1. Thus, the bandwidth allocation constraint can be expressed as

$$\sum_{i=1}^{I} \alpha_i[m] \leq 1 \quad \forall m. \tag{4}$$

Based on (3), one GT task U_i can have downlink data rate averagely as

$$r_i = \frac{1}{\sum_{m=1}^{M} t_m} \sum_{m=1}^{M} t_m r_i[m] \quad \forall i. \tag{5}$$

2) Computation Model: From the MEC server and central cloud, assume that the total computation capacity available for each UAV path line is $F_{\max}$ in CPU cycles, and the fraction of CPU cycle assigned to the MC of the ith GT in path line m is denoted by $f_i[m]$. Similar to $\alpha_i[m]$, it is known that when $F_{\max}$ is sufficiently large, $f_i[m]$ can be approximated to a continuous value between 0 and 1. Particularly, if the GT is controlled not to offload task to the UAV-enabled edge-cloud system in path line m, $f_i[m]$ is set to be 0. Thus, the computation capacity constraint is expressed as

$$\sum_{i=1}^{I} f_i[m] \leq 1 \quad \forall m. \tag{6}$$

Accordingly, during the whole UAV mission completion time, one GT task U_i has assigned computing capacity as

$$f_i^c = \sum_{m=1}^{M} f_i[m]F_{\max} \quad \forall i. \tag{7}$$

One has

$$f_i^c \leq F_{\max}^c \tag{8}$$

where $F^c_{\max}$ is the maximum allowed computation capacity allocated to a GT task from the MEC server and central cloud.

To offload a GT task U_i, the latency is formulated as

$$\frac{D_i}{r_i} + \frac{F_i}{f_i^c} \le T_i \quad \forall i \tag{9}$$

where it denotes that a GT task should be finished within its maximal allowed latency, and the overall latency includes the ones caused by data transmission and task computing in the MC of the GT.

We define $E_i[m]$ as the energy consumption of the UAV on computing task U_i in path line m, which is formulated as

$$E_i[m] = \varphi t_m (F_{\max} f_i[m])^{\vartheta} \tag{10}$$

where φ is the effective switched capacitance, and $\vartheta \ge 1$ is the positive constant [16], [22].

3) UAV Propulsion Energy Model: For a fixed-wing UAV, the propulsion energy is expressed as

$$E^{\text{f-uav}} = \sum_{m=1}^{M} t_m \left(c_1 \left(v_m^h\right)^3 + \frac{c_2}{v_m^h} + c_3 v_m^v \right) \tag{11}$$

where c_1 and c_2 are the two constant parameters related to the UAV's weight, wing area, and air density [15]; and c_3 is the constant parameter related to the UAV's descending/ascending. For a rotary-wing UAV, the propulsion energy is modeled as

$$E^{\text{r-uav}} = \sum_{m=1}^{M} t_m \left(P_0 \left(1 + \frac{3\left(v_m^h\right)^2}{U_{\text{tip}}^2} \right) + \frac{1}{2} d_0 \rho s G \left(v_m^h\right)^3 + P_1 \left(\sqrt{1 + \frac{\left(v_m^h\right)^4}{4\upsilon_0^4}} - \frac{\left(v_m^h\right)^2}{2\upsilon_0^2} \right)^{\frac{1}{2}} + P_2 v_m^v \right) \tag{12}$$

where P_0 and P_1 are two constants defined, representing the blade profile power and induced power in hovering status, respectively; and P_2 is the constant on descending/ascending power. U_{tip} denotes the tip speed of the rotor blade, v_0 is known as the mean rotor induced velocity in hover, d_0 and s are the fuselage drag ratio and rotor solidity, respectively, and ρ and G denote the air density and rotor disc area, respectively [14].

In general, the propulsion energy of UAV depends on the horizontal and vertical velocities of the UAV in each path segment. For the purpose of exposition and more tractable analysis, we ignore the additional/fewer energy consumption caused by UAV acceleration/deceleration, which is reasonable for scenarios when the UAV maneuvering duration only takes a small portion of the total operation time. In addition, the propulsion energy on UAV ascending/descending adopts a simple way, and an advanced model will be explored in our future work.

B. Problem Formulation

The optimization problem in this article is to minimize the overall energy consumption of the UAV-enabled MEC on service and UAV propulsion, while guaranteeing the service requirements of each GT task. Let $\mathbf{A} = \{\alpha_i[m], i \in \mathcal{I} \quad \forall m\}$, $\mathbf{P} = \{p_i[m], i \in \mathcal{I} \quad \forall m\}$, $\mathbf{F} = \{f_i[m], i \in \mathcal{I} \quad \forall m\}$, $\mathbf{Q} = \{q_m\}_{m=1}^{M+1}$, $\mathbf{H} = \{h_m\}_{m=1}^{M+1}$, and $\mathbf{T} = \{t_m\}_{m=1}^{M}$. The problem is then formulated as

$$\mathcal{P}: \min_{\mathbf{A},\mathbf{P},\mathbf{F},\mathbf{Q},\mathbf{H},\mathbf{T}} \left(E^{\text{uav}} + \beta \sum_{i=1}^{I} \sum_{m=1}^{M} (E_i[m] + \gamma t_m p_i[m]) \right) \tag{13}$$

$$\text{s.t.:} \quad \sum_{i=1}^{I} \alpha_i[m] \le 1 \quad \forall m \tag{13a}$$

$$\sum_{i=1}^{I} f_i[m] \le 1 \quad \forall m \tag{13b}$$

$$f_i^c \le F_{\max}^c \quad \forall i \tag{13c}$$

$$\frac{D_i}{r_i} + \frac{F_i}{f_i^c} \le T_i \quad \forall i \tag{13d}$$

$$\sum_{i=1}^{I} p_i[m] \le P_{\max} \quad \forall m \tag{13e}$$

$$\sum_{m=1}^{M} t_m \le T_{\max} \tag{13f}$$

$$\{q_1, h_1\} = \{q_{M+1}, h_{M+1}\} \tag{13g}$$

$$V_{\min}^h \le \frac{\|q_{m+1} - q_m\|}{t_m} \le V_{\max}^h, \quad m = 1, \ldots, M$$

$$0 \le \frac{\|h_{m+1} - h_m\|}{t_m} \le V_{\max}^v, \quad m = 1, \ldots, M \tag{13h}$$

$$\|q_{m+1} - q_m\| \le \Delta_{\max}^h, \quad m = 1, \ldots, M \tag{13i}$$

$$\|h_{m+1} - h_m\| \le \Delta_{\max}^v, \quad m = 1, \ldots, M \tag{13j}$$

$$h_{\max} \ge h_m \ge h_{\min} \quad \forall m \tag{13k}$$

where $E^{\text{uav}} = E^{\text{f-uav}}$ for fixed-wing UAV, and $E^{\text{uav}} = E^{\text{r-uav}}$ for rotary-wing UAV; $\beta > 0$ is the tradeoff between the energy consumptions of UAV on service and propulsion; $\gamma > 0$ is the tradeoff between the energy consumptions on computing and communication of a GT task; (13a) is the constraint on the allocation of the bandwidth; (13b) and (13c) are the constraints on the allocation of the computation capacity; (13d) is the constraint on the service requirement of each task on latency; (13e) is the constraint on the allocation of downlink transmitting power from UAV to GTs; and (13f)–(13l) are the constraints on UAV flight while both considering the UAV in the rotary-wing and fixed-wing styles.

According to $\mathcal{P}$, the allocations of bandwidth and computation capacities are highly correlated, which make the resource allocation nonconvex and become a multiple constrained optimization problem as shown in (13d). On the other hand, it is nonconvex to optimize UAV trajectory in terms of its locations in the horizontal and vertical dimensions. This is because the locations of UAV in both of the two dimensions are jointly constrained with respect to the LoS probabilities as defined in (1), and the velocities of the UAV in both dimensions should neither be too fast nor too slow to save propulsion energy as demonstrated in (11) and (12). Moreover, it is an NP-hard problem to jointly optimize the UAV trajectory and resource allocations, as the velocity and position of UAV will

affect the energy consumption of the UAV-enabled MEC on services. For example, if the velocity of the UAV is slow leading to longer t_m, it will cost less energy on service. On the other hand, if the velocity is fast leading to a shorter t_m of each path line m, the UAV needs to distribute more resources and consume more energy to finish the GT tasks. In the worst case, if t_m is too short, it is likely that the UAV-enabled MEC cannot provide satisfying services to GTs. According to the analysis, we generally find it is difficult to solve $\mathcal{P}$ in its current form.

III. Proposed Solution

To solve problem $\mathcal{P}$, we intend to optimize the resource allocation and UAV trajectory iteratively through a block coordinate descent method to reach a suboptimal solution iteratively. In each iteration, we first resolve the resource allocation problem with predefined UAV trajectory $\mathbf{Q}, \mathbf{H}, \mathbf{T}$. Afterward, we optimize the UAV trajectory given the resource allocation results $\mathbf{A}, \mathbf{P}$, and $\mathbf{F}$. When the block coordinate descent procedure converges to a predescribed accuracy, a suboptimal solution of $\mathcal{P}$ then can be found. This is similar to the SCO solution as proposed in [44] and [45], which can decrease the complicity of the original problem.

A. Optimize Resource Allocation With Predefined UAV Trajectory

Given predefined UAV trajectory, the optimization problem on resource allocation can be simplified as

$$\min_{\mathbf{A},\mathbf{P},\mathbf{F}} \sum_{i=1}^{I}\sum_{m=1}^{M}(E_i[m]+\gamma t_m p_i[m]) \quad \text{s.t.} \quad (13a)-(13e) \tag{14}$$

where the problem is nonconvex and cannot be solved directly due to nonconvex constraint (13d). To release the nonconvexity, we can convert (13d) to

$$f_i^c \geq \frac{F_i}{T_i - \frac{D_i}{r_i}} \quad \forall i \tag{15}$$

and given that $T_i > 0$, $f_i^c > 0$, one can get the minimum achievable rate as

$$r_i \geq R_i \quad \forall i \tag{16}$$

where

$$R_i = \frac{D_i}{T_i - \frac{F_i}{f_i^c}} \quad \forall i. \tag{17}$$

Then, (13d) can be reformulated into a tractable form as

$$\sum_{m=1}^{M} t_m \alpha_i[m] \log_2\left(1+\kappa_{im}\frac{p_i[m]}{\alpha_i[m]}\right) \geq R_i' \tag{18}$$

where $\kappa_{im} = [10^{[-(Ap_m^{\text{los}}+C)/10]}/BN_0(h_m^2+d_{im}^2)]$; $R_i' = [(\sum_{m=1}^{M} t_m)/B]R_i$. To this end, a subproblem of (14) can be defined as

$$\min_{\mathbf{A},\mathbf{P}} \left(\gamma \sum_{i=1}^{I}\sum_{m=1}^{M} t_m p_i[m]\right) \quad \text{s.t.} \quad (18);\ (13a);\ (13e) \tag{19}$$

where the problem is to optimize the allocation of the communication resource and the transmitting power $\mathbf{A}, \mathbf{P}$, given the allocation of computation capacity $\mathbf{F}$ determined already.

On the other hand, if $\mathbf{A}, \mathbf{P}$ determined, the problem on the allocation of computation capacity $\mathbf{F}$ becomes a linear program (LP) problem as defined as

$$\min_{\mathbf{F}} \sum_{i=1}^{I}\sum_{m=1}^{M} \varphi t_m (F_{\max} f_i[m])^{\vartheta} \quad \text{s.t.} \quad (15);\ (13b);\ (13c). \tag{20}$$

Based on (19) and (20), the resource allocation algorithm thus can be defined as an SCO procedure as demonstrated in Algorithm 1. In the algorithm, if we solve problems (19) and (20) separately in each iteration, the suboptimal results $\mathbf{A}$, $\mathbf{P}$, $\mathbf{F}$ will be obtained after the algorithm converging at a prescribed accuracy.

Obviously, the LP problem in (20) can be easily solved using the CVX tool [40]. However, it is difficult to solve (19) to jointly obtain **A, P** in Algorithm 1. In the following part, we leverage the Lagrange duality technique to handle the difficulty.

To convert (19) into a Lagrange duality problem, we reformulate it as

$$\min_{\mathbf{A},\mathbf{P},\boldsymbol{\omega}} \ \omega \quad \text{s.t.} \quad (18);\ (13a);\ (13e);\ \sum_{m=1}^{M} t_m p_i[m] \leq \omega \tag{21}$$

where ω is the maximal transmission power spent by the UAV to serve one GT task, i.e., $\omega \triangleq \max_{\forall i \in \mathcal{I}} \sum_{m=1}^{M}(t_m p_i[m])$. Equation (21) is convex and its Slater's constraint qualification is satisfied under its constraints that are either jointly convex or affine with respect to the variables **A, P**. Particularly, because of the predefined set of UAV trajectory, the sequence of UAV locations q_m, UAV height h_m, LoS probability p_m^{los}, and GT locations w_i are all fixed. κ_{im} in (18) therefore is constant. Define $\alpha_i[m]\log_2(1+\kappa_{im}(p_i[m]/\alpha_i[m])) \triangleq 0$ when $\alpha_i[m]=0$, r_i as the left-hand side of (18) is thus continuous and concave with respect to $\alpha_i[m]$ and $p_i[m]$ over the whole domain $0 \leq \alpha_i[m] \leq 1$ and $0 \leq p_i[m] \leq 1$. When the strong duality

Algorithm 1: Resource Allocation Given UAV Trajectory

```
Input: Q, H, T, j = 0, F^0;
repeat
    Obtain A^{j+1}, P^{j+1} by solving (19), given F^j;
    Obtain F^{j+1} by solving (20) using the CVX tool,
    given A^{j+1}, P^{j+1};
    j = j + 1;
until Converge to a prescribed accuracy;
```

holds in (21), the Lagrange function of the dual problem can be formulated as

$$\begin{aligned}\mathcal{L}(\mathbf{A},\mathbf{P},\boldsymbol{\omega},\lambda,\mu,\xi,\tau)&=\omega+\sum_{i=1}^{I}\lambda_i\left(\sum_{m=1}^{M}t_m p_i[m]-\omega\right)+\sum_{m=1}^{M}\mu_m\left(\sum_{i=1}^{I}\alpha_i[m]-1\right)\\&+\sum_{i=1}^{I}\xi_i\left(R_i'-\sum_{m=1}^{M}t_m\alpha_i[m]\log_2\left(1+\kappa_{im}\frac{p_i[m]}{\alpha_i[m]}\right)\right)\\&+\sum_{m=1}^{M}\tau_m\left(\sum_{i=1}^{I}p_i[m]-P_{\max}\right)\end{aligned}\tag{22}$$

where $\mu=\{\mu_m \quad \forall m\}$, $\tau=\{\tau_m \quad \forall m\}$, $\xi=\{\xi_i \quad \forall i\}$ and $\lambda=\{\lambda_i \quad \forall i\}$ are the nonnegative Lagrange multipliers associated with the constraints, respectively. In the duality function, because ω is not set with any upper boundary, it possibly has $\omega\to+\infty$. In order to make $\mathcal{L}(\mathbf{A},\mathbf{P},\boldsymbol{\omega},\lambda,\mu,\xi,\tau)$ bounded, i.e., $\mathcal{L}(\mathbf{A},\mathbf{P},\boldsymbol{\omega},\lambda,\mu,\xi,\tau)>-\infty$ and $\mathcal{L}(\mathbf{A},\mathbf{P},\boldsymbol{\omega},\lambda,\mu,\xi,\tau)<+\infty$, $(1-\sum_{i=1}^{I}\lambda_i)\omega=0$ must be hold. Therefore, we have $(1-\sum_{i=1}^{I}\lambda_i)=0$ as an additional constraint to the duality function. As such, the duality function of (21) is given by

$$\begin{aligned}&\mathcal{D}(\lambda,\mu,\xi,\tau)=\min_{\mathbf{A},\mathbf{P},\boldsymbol{\omega}}\mathcal{L}(\mathbf{A},\mathbf{P},\boldsymbol{\omega},\lambda,\mu,\xi,\tau)\\&\text{s.t.}\left(1-\sum_{i=1}^{I}\lambda_i\right)=0,\quad \tau\succeq 0;\mu\succeq 0;\xi\succeq 0;\lambda\succeq 0.\end{aligned}\tag{23}$$

Then, the duality problem is given by

$$\begin{aligned}&\max_{\lambda,\mu,\xi,\tau}\quad \mathcal{D}(\lambda,\mu,\xi,\tau)\\&\text{s.t.}\quad \left(1-\sum_{i=1}^{I}\lambda_i\right)=0,\quad \tau\succeq 0;\mu\succeq 0;\xi\succeq 0;\lambda\succeq 0.\end{aligned}\tag{24}$$

To obtain the duality function in (23), it involves the following:

$$\begin{aligned}&\min_{p_i[m],\alpha_i[m]}\quad (\tau_m+\lambda_i t_m)p_i[m]+\mu_m\alpha_i[m]\\&\qquad-\xi_i\left(t_m\alpha_i[m]\log_2\left(1+\kappa_{im}\frac{p_i[m]}{\alpha_i[m]}\right)\right)\\&\text{s.t.}\quad \left(1-\sum_{i=1}^{I}\lambda_i\right)=0,\quad \tau\succeq 0;\mu\succeq 0;\xi\succeq 0;\lambda\succeq 0\end{aligned}\tag{25}$$

where the subproblem is convex with respect to $p_i[m]$ and $\alpha_i[m]$. This is because $\alpha_i[m]\log_2(1+\kappa_{im}(p_i[m]/\alpha_i[m]))$ is jointly concave with respect to $p_i[m]$ and $\alpha_i[m]$. Therefore, the solutions that satisfy the Karush–Kuhn–Tucker (KKT) conditions are also the optimal solutions to (25). By taking the derivative of the objective function of (25) with respect to $p_i[m]$, the optimal allocation of transmission power, denoted by $p_i^*[m]$, can be obtained by solving the equation as

$$p_i^*[m]=\alpha_i[m]\left[\frac{\xi_i t_m}{(\tau_m+\lambda_i t_m)\ln 2}-\frac{1}{\kappa_{im}}\right]^+\tag{26}$$

where $[x]^+\triangleq\max\{0,x\}$. Let $\widetilde{p}_i[m]\triangleq(p_i^*[m]/\alpha_i[m])=[([\xi_i t_m]/[(\tau_m+\lambda_i t_m)\ln 2])-(1/\kappa_{im})]^+$, and it can be regarded as the power spectrum density of the ith GT when the UAV in path line m [46]. Substituting the obtained $p_i^*[m]$ into (26) yields

$$\begin{aligned}&\min_{\alpha_i[m]}\quad \alpha_i[m]\big((\tau_m+\lambda_i t_m)\widetilde{p}_i[n]+\mu_m-\xi_i t_m\log_2(1+\kappa_{im}\widetilde{p}_i[m])\big)\\&\text{s.t.}\quad \left(1-\sum_{i=1}^{I}\lambda_i\right)=0,\quad \tau\succeq 0;\mu\succeq 0;\xi\succeq 0;\lambda\succeq 0.\end{aligned}\tag{27}$$

Obviously, (27) is an LP problem on variable $\alpha_i[m]$. Thus, according to the monotonicity of this objective function, the optimal bandwidth allocation, denoted by $\alpha_i^*[m]$ can be obtained as

$$\alpha_i^*[m]=\begin{cases}1, & \text{if } c<0\\ b, & \text{if } c=0\\ 0, & \text{otherwise}\end{cases}\tag{28}$$

where $c=(\tau_m+\lambda_i t_m)\widetilde{p}_i[n]+\mu_m-\xi_i t_m\log_2(1+\kappa_{im}\widetilde{p}_i[m])$. In (28), b can be any arbitrary real number between 0 and 1 since the objective value of problem (28) is not affected in this case. For simplicity, we set $b=0$ as for the case.

After we find ($\mathbf{A}^*$,$\mathbf{P}^*$) through (28) and (26), the dual function $\mathcal{D}(\lambda,\mu,\xi,\tau)$ is obtained. Then, we are able to further solve the dual problem in (24) to obtain the optimal solution. We can use the projected subgradient method [39] to find the optimal dual variables, which are updated via iterations as

$$\mu_m^{(k+1)}=\left[\mu_m^k+s_k\underbrace{\left(\sum_{i=1}^{I}\alpha_i^k[m]-1\right)}_{g_1}\right]^+\quad\forall m\tag{29a}$$

$$\tau_m^{(k+1)}=\left[\tau_m^k+s_k\underbrace{\left(\sum_{i=1}^{I}p_i^k[m]-P_{\max}\right)}_{g_2}\right]^+\quad\forall m\tag{29b}$$

$$\xi_i^{(k+1)}=\left[\xi_i^k+s_k\underbrace{\left(R_i'-\sum_{m=1}^{M}t_m\alpha_i^k[m]\log_2\left(1+\kappa_{im}\frac{p_i^k[m]}{\alpha_i^k[m]}\right)\right)}_{g_3}\right]^+\quad\forall i\tag{29c}$$

$$\lambda_i^{(k+1)}=\left[\lambda_i^k+s_k\underbrace{\left(\sum_{m=1}^{M}t_m p_i^k[m]-\omega^k\right)}_{g_4}\right]^+\quad\forall i\tag{29d}$$

where $s_k>0$ is the step size of the kth iteration, which is configured to be $s_k=\gamma/\|g^k\|$; and g^k is the current obtained gradient of the dual function $\mathcal{D}(\lambda^k,\mu^k,\xi^k,\tau^k)$ in the kth iteration [39]. Specifically, in (29), g_1, g_2, g_3, and g_4 are the gradients of the dual function $\mathcal{D}(\lambda^k,\mu^k,\xi^k,\tau^k)$ with respect to μ^k, τ^k, ξ^k, and λ^k. Based on the Lagrange duality and projected subgradient method, we thus can give the iterative algorithm as shown in Algorithm 2, where the iterations converges to $\mathcal{D}^*$ when $\|\mathcal{D}^k-\mathcal{D}^*\|$ is smaller than some threshold.

Algorithm 2: Obtain **A**,**P** Through Projected Subgradient Method

Initialize $(\lambda, \mu, \xi, \tau)^1$, $k = 0$, $\mathcal{D}^0$=Inf;
repeat
  Update $\mathbf{P}^k$, $\mathbf{A}^k$ according to (26) and (28);
  Update $\mathcal{D}^k = \mathcal{D}\left(\lambda^k, \mu^k, \xi^k, \tau^k\right)$ by (23);
  Update $(\lambda, \mu, \xi, \tau)^{k+1}$ by (29), $k = k + 1$;
until $(\mathcal{D}^{(k-1)} - \mathcal{D}^k) \leq \Delta\mathcal{D}$;

However, because $\|\mathcal{D}^k - \mathcal{D}^*\|$ decreases very slowly [39], the subgradient method in Algorithm 2 is usually used without any formal stopping criterion, but a fairly and affordable number of iterations. Based on this idea, we assume Algorithm 2 coverages at the kth iteration, if the value of the dual function in the kth iteration is not larger enough than the dual value in the previous iteration, i.e., $(D^k - D^{(k-1)}) \leq \Delta\mathcal{D}$. Then, the obtained $\mathbf{A}^{k-1}$, $\mathbf{P}^{k-1}$ are set to be optimal solution of (23).

Through Algorithm 2, we can get the optimized resource allocation as (**A**, **P**). However, **A** obtained may not be feasible to problem (21). This is because one $\alpha_i[n]$ calculated by (28) is not unique, when $(\tau_m + \lambda_i t_m)\widetilde{p}_i[n] + \mu_m - \xi_i t_m \log_2(1 + \kappa_{im}\widetilde{p}_i[m]) = 0$. In order to find feasible **A**, we can redefine problem (19) as

$$\min_{\mathbf{A}} \left(\gamma \sum_{i=1}^{I}\sum_{m=1}^{M} t_m \widetilde{p}_i^*[m]\alpha_i[m]\right) \text{ s.t. (13a); (13e)}$$
$$\sum_{m=1}^{M} t_m \log_2\left(1 + \kappa_{im}\widetilde{p}_i^*[m]\right)\alpha_i[m] \geq R_i' \tag{30}$$

where $\widetilde{p}_i^*[n]$ is the constant and has been uniquely obtained through the projected subgradient method in Algorithm 2. Obviously, (30) is an LP problem. We can solve the problem using convex optimization tool, like CVX, to obtain the feasible **A**. Afterward, we recalculate **P** as $p_i[m] = \widetilde{p}_i^*[m]\alpha_i[m] \quad \forall i, m$. Then (19) is finally solved.

B. Optimize UAV Trajectory Given Resource Allocations

With predetermined **A**, **P**, and **F**, the problem on optimizing the trajectory of the rotary-wing and fixed-wing UAVs can be separately formulated as

$$\min_{\mathbf{Q},\mathbf{H},\mathbf{T}} \sum_{m=1}^{M} t_m \left(P_0\left(1 + \frac{3\left(v_m^h\right)^2}{U_{\text{tip}}^2}\right) + \frac{1}{2}d_0\rho s G\left(v_m^h\right)^3 + P_1\left(\sqrt{1 + \frac{\left(v_m^h\right)^4}{4\upsilon_0^4}} - \frac{\left(v_m^h\right)^2}{2\upsilon_0^2}\right)^{\frac{1}{2}} + P_2 v_m^v \right)$$
$$\text{s.t.} \quad \text{(13d); (13f)}-\text{(13l)} \tag{31}$$

$$\min_{\mathbf{Q},\mathbf{H},\mathbf{T}} \sum_{m=1}^{M} t_m \left(c_1\left(v_m^h\right)^3 + \frac{c_2}{v_m^h} + c_3 v_m^v \right)$$
$$\text{s.t.} \quad \text{(13d); (13f)}-\text{(13l)}. \tag{32}$$

The nonconvex problem in (31) and (32) works on the energy model of the rotary-wing and fixed-wing UAVs separately, which are complicated and cannot be solved directly. For a specific type of UAV, we intend to release the nonconvexities and divide the problem into three subproblems on horizontal trajectory **Q**, vertical locations **H**, and flight time **T**, respectively. The obtained convex subproblems then can be directly solved through an SCO procedure.

1) Optimize Horizontal Trajectory of Rotary-Wing UAV: Given **H** and **T**, the problem on optimizing horizontal trajectory **Q** of rotary UAV can be formulated as

$$\min_{\mathbf{Q}} \sum_{m=1}^{M} t_m \left(P_0\left(1 + \frac{3\left(v_m^h\right)^2}{U_{\text{tip}}^2}\right) + \frac{1}{2}d_0\rho s G\left(v_m^h\right)^3 + P_1\left(\sqrt{1 + \frac{\left(v_m^h\right)^4}{4\upsilon_0^4}} - \frac{\left(v_m^h\right)^2}{2\upsilon_0^2}\right)^{\frac{1}{2}} \right)$$
$$\text{s.t.} \quad \text{(13d); (13g); (13h); (13j).} \tag{33}$$

To further simplify (33), we introduce slack variables $\phi_m = (\sqrt{1 + [(v_m^h)^4/4\upsilon_0^4]} - [(v_m^h)^2/2\upsilon_0^2])^{(1/2)}$, which are equivalent to $(1/\phi_m^2) = \phi_m^2 + [(v_m^h)^2/\upsilon_0^2]$. Let $E_m^{\phi} \triangleq t_m(P_0(1 + [(3(v_m^h)^2)/(U_{\text{tip}}^2)] + (1/2)d_0\rho s G(v_m^h)^3 + P_1\phi_m)$, then as proofed in [11], (33) can be equivalently reformed as

$$\min_{\mathbf{Q},\boldsymbol{\phi}_\mathbf{m}} \sum_{m=1}^{M} E_m^{\phi} \tag{34}$$
$$\text{s.t.} \quad \text{(13d); (13g); (13h); (13j)}$$
$$\phi_m^2 + \frac{\left(v_m^h\right)^2}{\upsilon_0^2} \geq \frac{1}{\phi_m^2}. \tag{34a}$$

The problem in (34) is still nonconvex due to the nonconvex terms in (13d), (13h), and (34a). We first relax (13d) to have

$$\sum_{m=1}^{M} t_m \alpha_i[m] \log_2\left(1 + \frac{p_i[m]10^{\frac{-l_{im}}{10}}}{\alpha_i[m]BN_0}\right) \geq R_i' \tag{35}$$

where $R_i' = ([\sum_{m=1}^{M} t_m D_i]/[B(T_i - [F_i/f_i^c])])$. Then, if we bring (2) into the left-hand side of (35), one has

$$\sum_{m=1}^{M} t_m \alpha_i[m] \log_2\left(1 + \frac{p_i[m]}{\alpha_i[m]} \frac{10^{-\frac{Ap_{im}^{\text{los}} + C}{10}}}{BN_0\left(h_m^2 + d_{im}^2\right)}\right)$$
$$\geq \sum_{m=1}^{M} t_m \alpha_i[m] \log_2\left(1 + \frac{p_i[m]}{\alpha_i[m]} \frac{10^{-\frac{C}{10}}}{BN_0} \frac{1}{h_m^2 + d_{im}^2}\right) \tag{36}$$

where the inequality is due to $p_{im}^{\text{los}} \geq 0$ and $A < 0$, i.e., $\eta_{\text{LoS}} < \eta_{\text{NLoS}}$. Then, (35) is simplified as

$$\sum_{m=1}^{M} t_m \alpha_i[m] \log_2(1 + \xi_{im} f(d_{im})) \geq R_i' \tag{37}$$

where $\xi_{im} = [(p_i[m])/(\alpha_i[m])][(10^{-[C/10]})/(h_m^2 BN_0)]$, and $f(x) = (1/[1 + (x^2/h_m^2)])$. In (37), the left-hand side of the inequality is still nonconvex to d_{im}. It motivates us to replace this nonconvexity by more tractable convex function derived from the Taylor expansion at a given local point [37].

Specifically, with given local point d_{im}^l, we have the following inequality:

$$\sum_{m=1}^{M} t_m \alpha_i[m] \log_2(1+\xi_{im} f(d_{im})) \geq \sum_{m=1}^{M} t_m \alpha_i[m] \left(A_{im}^l \left(d_{im} - d_{im}^l \right) + B_{im}^l \right) \tag{38}$$

where

$$A_{im}^l = \frac{-2\xi_{im} \frac{d_{im}^l}{h_m^2}}{\ln 2 \left(\left(1 + \left(\frac{d_{im}^l}{h_m} \right)^2 \right)^2 + \xi_{im} \left(1 + \left(\frac{d_{im}^l}{h_m} \right)^2 \right) \right)}$$

$$B_{im}^l = \log_2 \left(1 + \xi_{im} f \left(d_{im}^l \right) \right).$$

The local point d_{im}^l is directly obtained given the current status of the horizontal trajectory $\{q_{m+1}^l, q_m^l\}$ of the UAV. Then, (13d) finally can be expressed into linear form as

$$\sum_{m=1}^{M} t_m \alpha_i[m] \left(A_{im}^l \left(d_{im} - d_{im}^l \right) + B_{im}^l \right) \geq R_i'. \tag{39}$$

Second, consider nonconvex (34a), at the given local points ϕ_m^l and $\hat{v}_m^h$ that are obtained following the current status of the UAV, we can apply the first-order Taylor expansion to ϕ_m as

$$\phi_m^4 + \phi_m^2 \frac{\left(v_m^h\right)^2}{\upsilon_0^2} \geq X_m^{bl} = \left(4 \left(\phi_m^l \right)^3 + 2\phi_m^l \frac{\left(\hat{v}_m^h \right)^2}{\upsilon_0^2} \right) \phi_m - 3 \left(\phi_m^l \right)^4 - \frac{\left(\phi_m^l \hat{v}_m^h \right)^2}{\upsilon_0^2}. \tag{40}$$

Then, (34a) can be expressed into a linear form as

$$X_m^{bl} \geq 1. \tag{41}$$

Third, to make constraint (13h) tractable, one has to turn the left-hand side, i.e., $V_{\min}^h \leq \|q_{m+1} - q_m\|$, of the constraint into a linear format. To do so, at the given points $\{q_{m+1}^l, q_m^l\}$ as the current status of the horizontal trajectory of the UAV, we define the following inequality by applying the first-order Taylor expansion as:

$$\|q_{m+1} - q_m\|^2 \geq -\left\| q_{m+1}^l - q_m^l \right\|^2 + 2 \left(q_{m+1}^l - q_m^l \right)^T (q_{m+1} - q_m) = q_m^{\mathrm{bl}}. \tag{42}$$

Then, the left-hand side of constraint (13h) can be converted as

$$q_m^{\mathrm{bl}} \geq \left(t_m V_{\min}^h \right)^2. \tag{43}$$

Finally, due to all the nonconvex terms relaxed, (34) can be eventually redefined as a convex QCQP problem as

$$\min_{\mathbf{Q}, \boldsymbol{\phi}_{\mathbf{m}}} \sum_{m=1}^{M} E_m^{\phi} \tag{44}$$

$$\text{s.t.} \quad (13\text{g}); (39); (41); (43)$$

$$\|q_{m+1} - q_m\| \leq \min \left\{ \Delta_{\max}^h, t_m V_{\max}^h \right\} \tag{44a}$$

which can be solved directly by the CVX tool. Then, the suboptimal horizontal trajectory of the rotary-wing UAV $\mathbf{Q}$ can be successfully obtained.

2) Optimize Horizontal Trajectory of Fixed-Wing UAV: For fixed-wing UAV, given its current horizontal velocity $\hat{v}_m^h$ working as the local point, by applying the first-order Taylor expansion of the energy function in (32), one has

$$\frac{1}{t_m \left(c_1 \left(v_m^h \right)^3 + \frac{c_2}{v_m^h} \right)} \geq W_m^{bl} = \frac{-3c_1 \left(\hat{v}_m^h \right)^2 + \frac{c_2}{\left(\hat{v}_m^h \right)^2}}{t_m \left(c_1 \left(\hat{v}_m^h \right)^3 \frac{c_2}{\hat{v}_m^h} \right)^2} v_m^h + \frac{4c_1 \left(\hat{v}_m^h \right)^3}{t_m \left(c_1 \left(\hat{v}_m^h \right)^3 \frac{c_2}{\hat{v}_m^h} \right)^2}. \tag{45}$$

Then, with the same work to relax the nonconvex terms in (13d), (13h), and (34a) as in the last section, (32) can be modeled as

$$\max_{\mathbf{Q}} \ \min_{\forall m} \left(W_m^{bl} \right) \quad \text{s.t.} \quad (13\text{g}); (39); (43); (44\text{a}) \tag{46}$$

which is a QCQP problem, and can be solved directly by the CVX tool.

3) Optimize UAV Vertical Trajectory: Given $\mathbf{Q}$ and $\mathbf{T}$, the problem on optimizing the vertical trajectory $\mathbf{H}$ of both the rotary-wing and fixed-wing UAVs can be formulated as

$$\min_{\mathbf{H}} \ \max_{\forall m} \|h_{m+1} - h_m\| \tag{47}$$

$$\text{s.t.} \quad (13\text{g}); (13\text{i}); (13\text{k})$$

$$\hat{r}_i^{bl} \geq R_i' \quad \forall i \tag{47a}$$

where $\hat{r}_i^{bl} = \sum_{m=1}^{M} t_m \alpha_i[m] (Y_{im}^l (h_m - h_{im}^l) + Z_{im}^l)$ with

$$Y_{im}^l = \frac{-2\hat{\xi}_{im} \frac{h_m^l}{d_{im}^2}}{\ln 2 \left(\left(1 + \left(\frac{h_m^l}{d_{im}} \right)^2 \right)^2 + \hat{\xi}_{im} \left(1 + \left(\frac{h_m^l}{d_{im}} \right)^2 \right) \right)}$$

$$Z_{im}^l = \log_2 \left(1 + \hat{\xi}_{im} \hat{f} \left(h_m^l \right) \right)$$

$$\hat{f}(x) = \frac{1}{1 + \frac{x^2}{d_{im}^2}} \quad \hat{\xi}_{im} = \frac{p_i[m]}{\alpha_i[m]} \frac{10^{-\frac{C}{10}}}{d_{im}^2 B N_0}.$$

Obviously, in (47a), $\hat{r}_i^{bl}$ is obtained following the identical procedure as the one applied in (36)–(39), while taking $h_m \quad \forall m$ as the variables. It can be found that (47) is a QCQP problem to control UAV to approach SLF to minimize the propulsion energy in the vertical dimension, while ensuring acceptable task latency for GTs. Thus, (47) can be solved directly by the CVX tool.

4) Optimize UAV Flight Time: Given $\mathbf{Q}$ and $\mathbf{H}$, the problem on optimizing flight time $\mathbf{T}$ of both the rotary-wing and fixed-wing UAVs in each path line can be formulated as

$$\min_{\mathbf{T}} \max_{\forall m} \left\| \left(t_m v_h^* \right)^2 - \|q_{m+1} - q_m\|^2 \right\| \tag{48}$$

$$\text{s.t.} \quad (13\text{f}); (13\text{h}); (13\text{i})$$

Algorithm 3: Optimize UAV Trajectory Given Resource Allocations

1 Input: $\mathbf{A}$, $\mathbf{P}$, $\mathbf{F}$, $j=0$; $\mathbf{Q}^j=\mathbf{Q}$, $\mathbf{H}^j=\mathbf{H}$, $\mathbf{T}^j=\mathbf{T}$, θ;
2 **repeat**
3 Obtain $\mathbf{Q}^{j+1}$ by solving (44) for the rotary-wing UAV, or (46) for the fixed-wing UAV, with given $\mathbf{H}^j$, $\mathbf{T}^j$;
4 Obtain $\mathbf{H}^{j+1}$ by solving (47), given $\mathbf{Q}^{j+1}$, $\mathbf{T}^j$;
5 Obtain $\mathbf{T}^{j+1}$ by solving (48), given $\mathbf{Q}^{j+1}$, $\mathbf{H}^{j+1}$;
6 $j=j+1$;
7 **until** *Converge to a prescribed accuracy*;

$$\sum_{m=1}^{M} t_m \le \sum_{m=1}^{M} t_m^l \tag{48a}$$

$$\sum_{m=1}^{M} t_m r_{im} \ge \frac{\sum_{m=1}^{M} t_m^l}{B} R_i \tag{48b}$$

where $r_{im}=\alpha_i[m]\log_2(1+[(p_i[m]10^{(-l_{im}/10)})/(\alpha_i[m]BN_0)])$; (48a) denotes the UAV flight time should be decreased to lower than the current time $\sum_{m=1}^{M} t_m^l$ to save the overall propulsion energy. By bring (48a) into (5), one can have $r_i \ge (B/\sum_{m=1}^{M} t_m^l)\sum_{m=1}^{M} t_m r_{im}$. Thus, constraint (13d) on GT task latency can be converted to $(B/\sum_{m=1}^{M} t_m^l)\sum_{m=1}^{M} t_m r_{im} \ge R_i$, and denoted as (48b). In (48), v_h^* is the horizontal velocity in optimal that leads to the minimum of the propulsion power in the horizontal dimension. For fixed-wing UAV, by solving the convex expression of $E^{\text{f-uav}}$ in (11), a closed-form expression of v_h^* can be obtained as: $\min(\max(\sqrt[4]{(c_2/3c_1)}, V_{\min}^h), V_{\max}^h)$. For rotary-wing, v_h^* is difficult to obtain due to the complicated expression of $E^{\text{r-uav}}$ in (12), however, it can be efficiently found numerically [14]. Obviously, (48) is to optimize the duration time t_m of the UAV in each path line to let the UAV approaching the optimal horizontal speed v_h^*. With the optimized $\mathbf{T}$, the UAV could have minimized propulsion energy, while ensuring the GT tasks finished before deadline. In addition, it can be noted in (11) and (12), that we simply assume the propulsion energy in the vertical dimension only correlates to the distance on UAV descending/ascending. The optimization of the flight time in (48) thus does not take the acceleration/deceleration of the UAV in the vertical dimension into consideration. As discussed in the system model, we intend to realize the optimization considering the acceleration/deceleration of the UAV in future work.

5) Overall Algorithm on UAV Trajectory: Using the methods designed in the previous three sections, the overall algorithm to find the suboptimal UAV trajectory is designed as Algorithm 3. In each iteration of the algorithm, it sequentially solves the problems in (44), (46), (47), and (48) to update the trajectory of the rotary-wing or fixed-wing UAV to approach the optimal. As shown in steps 2–7, it tries to control the UAV to adopt SLF and the horizontal trajectory to consume as less propulsion energy as possible, while support satisfying task offloading. The algorithm will converge to a prescribed accuracy within finite iterations. Then, a desirable suboptimal UAV trajectory will be found.

Algorithm 4: Overall Algorithm

1 Initialize $i=0$, $\mathbf{Q}^0$, $\mathbf{H}^0$, $\mathbf{T}^0$;
2 **repeat**
3 Obtain $\mathbf{A}^i$, $\mathbf{P}^i$, $\mathbf{F}^i$ through Algorithm 1, given $\mathbf{Q}^i$, $\mathbf{H}^i$, $\mathbf{T}^i$;
4 Obtain $\mathbf{Q}^{i+1}$, $\mathbf{H}^{i+1}$, $\mathbf{T}^{i+1}$ through Algorithm 3, given $\mathbf{A}^i$, $\mathbf{P}^i$, $\mathbf{F}^i$;
5 $i=i+1$;
6 **until** *Converge to a prescribed accuracy*;

C. Overall Algorithm Design

Based on the solutions provided, the overall algorithm to find the suboptimal solution of $\mathcal{P}$ can be designed as in Algorithm 4, where in the beginning, the UAV trajectory is first initialized to have path line: $\{q_m^0\}_{m=1}^{M+1}$. We intend to initialize the UAV trajectory to let the UAV travel to each place of interest with the shortest distance. Such UAV trajectory can be found by solving the traveling salesman problem (TSP) [47]. Following the initialized path $\{q_m^0\}_{m=1}^{M+1}$, the UAV thus can fly geographically close to the GTs without considering the energy efficiency. Also, in the beginning, it assumes the UAV stays in each of the initialized path line segments in a fixed duration t_0 and flies with height $\{h_m^0\}_{m=1}^{M+1}$. After initialization, the algorithm mainly runs a loop with finite iterations from step 2 to step 6. In each iteration, it solves (14) to obtain $\mathbf{A}^i$, $\mathbf{P}^i$, $\mathbf{F}^i$ following Algorithm 1 at step 3. Afterward, the UAV trajectory can be updated to be $\mathbf{Q}^{i+1}$, $\mathbf{H}^{i+1}$, and $\mathbf{T}^{i+1}$ via Algorithm 3 with respect to $\mathbf{A}^i$, $\mathbf{P}^i$, and $\mathbf{F}^i$ at step 4. As the iterations going on, the overall energy consumption of the UAV will gradually descend. After the algorithm converging to a prescribed accuracy within finite iterations, a desirable suboptimal solution of problem $\mathcal{P}$ will be found.

D. Complexity and Convergence of the Overall Algorithm

Generally, in each iteration of Algorithm 3, the UAV horizontal trajectory, vertical trajectory, and flight time in each path line are sequentially optimized using the convex solver based on the interior-point method, and thus their individual complexity can be resented by $O((IM)^{3.5}\log(1/\epsilon))$, respectively, given the solution accuracy of $\epsilon > 0$ [48]. In Algorithm 1, the most effort is to optimize the resource variables $\mathbf{A}$, $\mathbf{P}$, and $\mathbf{F}$ in (14) using the Lagrange duality, then the time complexity can be denoted as $O(IM)$. Then accounting for the block coordinate descendant iterations of Algorithm 4 with the complexity in the order of $\log(1/\epsilon)$, the total computation complexity of Algorithm 4 is $O(IM)^{3.5}\log^2(1/\epsilon))$. In practice, the UAV-enabled MEC server and central cloud will well support the running of optimization solution under different GT scenarios. Also, because the UAV-enabled MEC is normally working in the sparse scenarios, where there is not too much GTs, the proposed optimized solution therefore is practical to be deployed.

Afterward, we concern the convergence of the proposed solution. First, let $\bar{E}(\mathbf{A}^i, \mathbf{F}^i, \mathbf{P}^i)$ denote the objective value of (14) in the ith iteration of Algorithm 1. Then, in the $(i+1)$th

iteration of Algorithm 1, one has

$$\bar{E}\left(\mathbf{A}^i, \mathbf{P}^i, \mathbf{F}^i\right) \overset{(a)}{\geq} \bar{E}\left(\mathbf{A}^{i+1}, \mathbf{P}^{i+1}, \mathbf{F}^i\right) \overset{(b)}{\geq} \bar{E}\left(\mathbf{A}^{i+1}, \mathbf{P}^{i+1}, \mathbf{F}^{i+1}\right) \tag{49}$$

where (a) and (b) hold based on the solving of (19) and (20). Therefore, the objective value of (14) is nonincreasing in Algorithm 1, and the algorithm can converge to a locally optimal solution of (14).

Second, we concern the convergence of Algorithm 3. Let $\hat{E}(\mathbf{Q}^i, \mathbf{H}^i, \mathbf{T}^i)$ denote the objective value of (31)/(32) in the ith iteration of Algorithm 3. Then, in the $(i+1)$th iteration of Algorithm 3, one has

$$\begin{aligned}\hat{E}\left(\mathbf{Q}^i, \mathbf{H}^i, \mathbf{T}^i\right) &\overset{(a)}{=} \hat{E}^{bl}\left(\mathbf{Q}^i, \mathbf{H}^i, \mathbf{T}^i\right) \overset{(b)}{\geq} \hat{E}\left(\mathbf{Q}^{i+1}, \mathbf{H}^i, \mathbf{T}^i\right) \\ &\overset{(d)}{=} \hat{E}^{bl}\left(\mathbf{Q}^{i+1}, \mathbf{H}^i, \mathbf{T}^i\right) \overset{(d)}{\geq} \hat{E}\left(\mathbf{Q}^{i+1}, \mathbf{H}^{i+1}, \mathbf{T}^i\right) \\ &\overset{(e)}{=} \hat{E}^{bl}\left(\mathbf{Q}^{i+1}, \mathbf{H}^{i+1}, \mathbf{T}^i\right) \overset{(f)}{\geq} \hat{E}\left(\mathbf{Q}^{i+1}, \mathbf{H}^{i+1}, \mathbf{T}^{i+1}\right)\end{aligned} \tag{50}$$

where (b), (d), and (f) hold, if problems in (44)/(46), (47), and (48) are sequentially solved. We can find that (a) and (c) hold, because we obtain $\mathbf{Q}^{i+1}$ and $\mathbf{H}^{i+1}$ by taking $\mathbf{Q}^i$ and $\mathbf{H}^i$ as the local points of the first-order Taylor expansions in (44)/(46) and (47). Further more, (e) holds because we obtain $\mathbf{T}^{i+1}$ by taking $\mathbf{T}^i$ as the benchmark local point in (48). Thus, it is validated that the objective value of (31)/(32) is nonincreasing in Algorithm 3, and the algorithm can converge to a locally optimal solution of the trajectory optimization problem.

Finally, to address the convergency of the overall algorithm (Algorithm 4), let $E(\mathbf{A}^i, \mathbf{P}^i, \mathbf{F}^i, \mathbf{Q}^i, \mathbf{H}^i, \mathbf{T}^i)$ denote the objective value of $\mathcal{P}$ in the ith iteration of Algorithm 4. Thus, one has $E(\mathbf{A}^i, \mathbf{P}^i, \mathbf{F}^i, \mathbf{Q}^i, \mathbf{H}^i, \mathbf{T}^i) = \bar{E}(\mathbf{A}^i, \mathbf{P}^i, \mathbf{F}^i) + \beta\hat{E}(\mathbf{Q}^i, \mathbf{H}^i, \mathbf{T}^i)$. Based on (49) and (50), we can easily get that $E(\mathbf{A}^i, \mathbf{P}^i, \mathbf{F}^i, \mathbf{Q}^i, \mathbf{H}^i, \mathbf{T}^i) > E(\mathbf{A}^{i+1}, \mathbf{P}^{i+1}, \mathbf{F}^{i+1}, \mathbf{Q}^{i+1}, \mathbf{H}^{i+1}, \mathbf{T}^{i+1})$. To this end, it is validated that the objective value of $\mathcal{P}$ is nonincreasing in Algorithm 4, and thus Algorithm 4 can converge to a locally optimal solution of problem $\mathcal{P}$.

IV. Simulation

In this section, the proposed solution is validated through simulation using MATLAB with the CVX tool. The simulation considers GT distributions in sparse, medium, and densified scenarios. These different scenarios are used to evaluate the adaptability of the proposed solution in contrast to other solutions. We consider that the UAV does not transmit data during landing and taking off. Hence, the UAV only supports the task offloading when they are airborne. Moreover, we assume that the initial and final locations are predetermined based on the mission objectives. We compare our optimized solution (OP) to two baseline solutions, i.e., BL-1 and BL-2. In specific, BL-1 aims to control UAV flying closer to GTs to facilitate the task offloading. BL-1 will allocate communication and computation resources to UAV–GT pairs in a water-filling method [49]. Thus, BL-1 is to let UAV finish the GT tasks as quickly as possible, while not considering energy efficiency nor resource efficiency of the UAV. On the contrary, BL-2 controls the UAV to fly in a near-optimal velocity that leads to the minimum propulsion energy in the horizontal dimension and adopts a close SLF in the vertical dimension. In addition, BL-2 allocates the communication and computation resources to UAV–GT pairs using the convex optimization method as proposed in Algorithm 1. Thus, BL-2 most worries about minimizing the energy of the UAV, but less the service requirement of GTs. According to our study, BL-1 and BL-2 are the recent state-of-the-art solutions that also use convex optimization to reach the near-optimal solution. Other solutions, like exhaustive search, genetic algorithm, and heuristic search, are computational impossible for the optimization problem of this article. Most recent, AI algorithms, like deep reinforcement learning [50], will not compared here as they have not been theoretically studied on this optimization problem yet. We set the parameters applied in the simulation as listed in Table I. The parameters on the air–ground communication are set based on the scenario discussed in [5]. The parameters on task settings and GT distributions are based on the scenario discussed in [23]. The parameters on the propulsion model are based on the settings in [14] for rotary-wing UAV and [15] for fixed-wing UAV. In general, the parameter settings on simulation are based on the realistic scenarios.

TABLE I
Parameter Settings on Simulation

Parameter	Value
Bandwidth B, DL power: $P_{\max}$	2GHz, 5W
Pathloss: a, b, η_{LoS}, η_{NLos}	9.61, 0.16, 1, 20 [5]
Fixed-wing: c_1, c_2, c_3	$9.26 * 10^{-4}$, 2250, 3.33 [15]
Rotary-wing:U_{tip},v_0,d_0,s, ρ, G	120, 4.3, 0.6, 0.05, 1.225, 0.503 [14]
P_0, P_1, P_2	$\frac{12*30^3*0.4^3}{8}\rho s G$, $\frac{1.1*20^{3/2}}{\sqrt{2\rho G}}$,11.46
$\Delta^h_{\max}$, $\Delta^v_{\max}$	35m, 20m
fixed-wing: $V^h_{\max}$, $V^h_{\min}$, $V^v_{\max}$	35m/s, 5m/s, 20m/s
Rotary-wing: $V^h_{\max}$, $V^h_{\min}$, $V^v_{\max}$	20m/s, 0m/s, 15m/s
Noisy density: N_0	-169dBm/Hz
Energy on computation: φ, ϑ	$10^{-9}, 3$
GT task:T_k, D_k	200∼300s, 40∼80 Mb
GT task: F_k	$1 \times 10^6 \sim 2 \times 10^6$ CPU cycles
$T_{\max}$, $\widehat{D}$	5 minutes, 3Km
$F_{\max}$, $F^c_{\max}$	2GHz, $F_{\max} \times M/K$
UAV height: h^0_m, $h_{\min}$, $h_{\max}$	100m, 50m, 300m
Number of GTs: K	7(sparse),21(medium),35(densified)

In Figs. 2 and 3, the UAV trajectory in the 3-D and 2-D spaces led by different solutions is demonstrated, where the UAV in fixed wing or rotary wing is initialized to fly a trajectory led by TSP in different GT scenarios. As shown in Figs. 2 and 3, BL-1 controls the UAV to fly geographically close to GTs for better UAV–GT links. BL-2 controls the UAV to adopt trajectories in a conservative way that intends to consume the least propulsion energy. In contrast, OP controls the UAV to fly neither too close nor too far wary from the GTs. Therefore, with OP, the UAV can better balance its energy

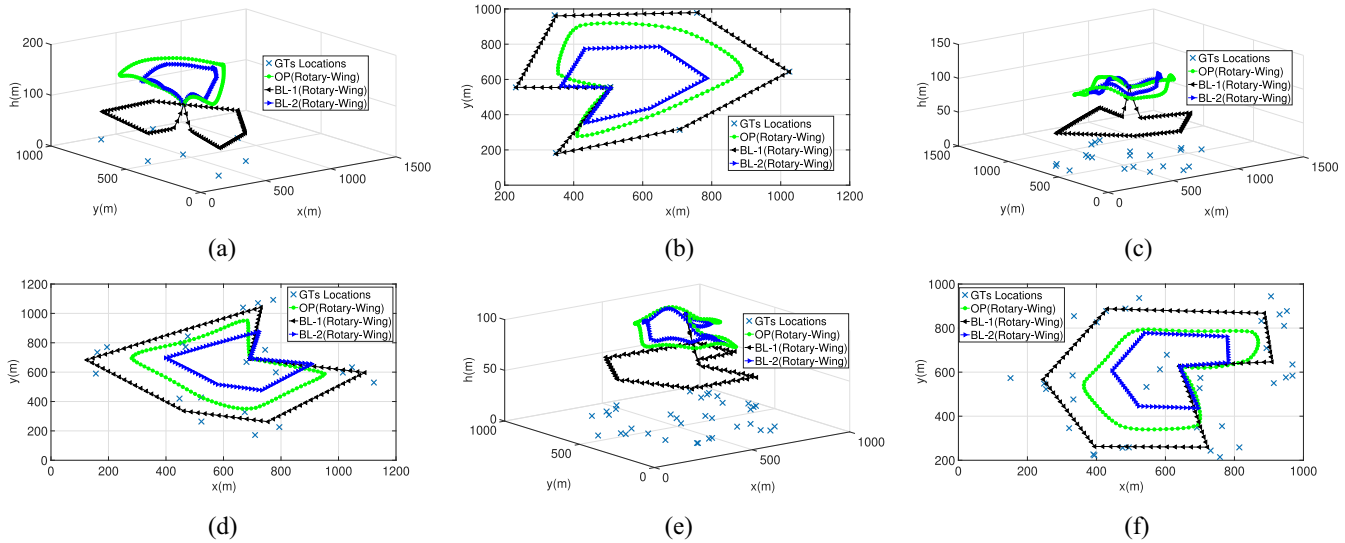

Fig. 2. Trajectory of rotary-wing UAV led by different solutions in sparse, medium, and densified scenarios: (a) 3-D, sparse scenario; (b) 2-D, sparse scenario; (c) 3-D, medium scenario; (d) 2-D, medium scenario; (e) 3-D, densified scenario; and (f) 2-D, densified scenario.

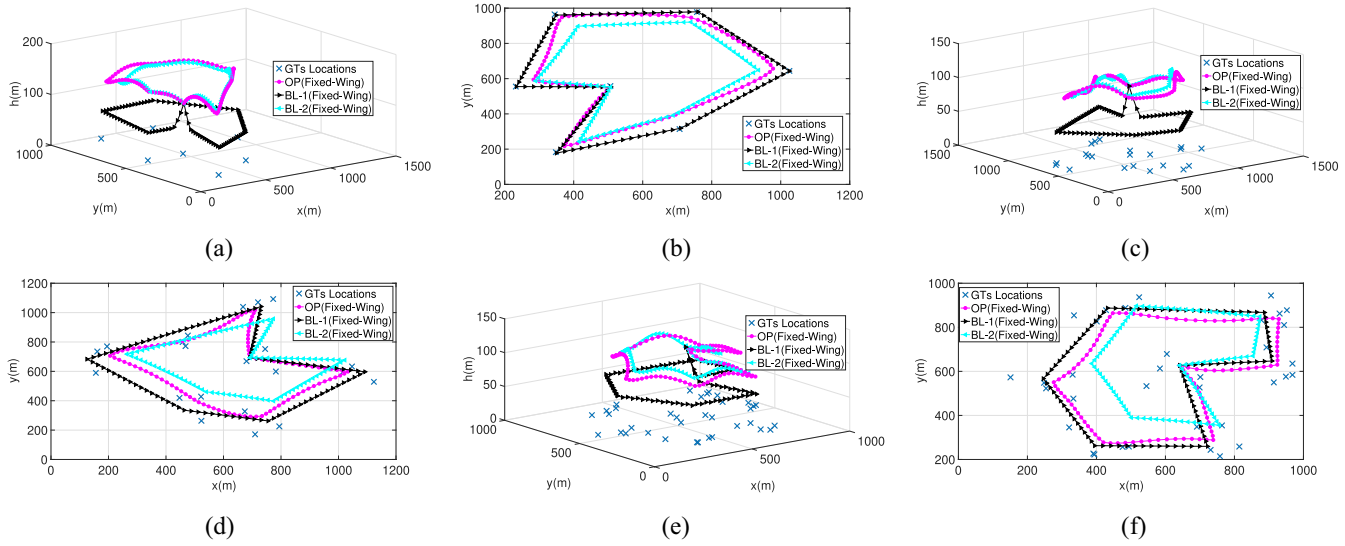

Fig. 3. Trajectory of fixed-wing UAV led by different solutions in sparse, medium, and densified scenarios: (a) 3-D, sparse scenario; (b) 2-D, sparse scenario; (c) 3-D, medium scenario; (d) 2-D, medium scenario; (e) 3-D, densified scenario; and (f) 2-D, densified scenario.

consumption and services to work with energy efficiency. In addition, Figs. 2 and 3 show that the fixed-wing UAV adopts a trajectory with a longer distance compared to the rotary-wing UAV. This is because the fixed-wing UAV cannot hover statically and requests a minimum velocity to stay aloft. On the other hand, in the vertical dimension, Figs. 2 and 3 show that the UAV normally ascends/descends from its original height to a better link to GTs. Compared to BL-1 that controls the UAV to descend/ascend dramatically, OP and BL-2 control the UAV to ascend/descend less distance in a smooth manner. OP and BL-2 thus help save the energy consumption of the UAV in the vertical dimension. Moreover, the rotary-wing UAV will have longer flight time in each discrete time slot, as the UAV can hover statically at specific locations. Due to the limited space of this article, we do not provide the related numerical results on flight time in this article.

To validate the effect of different solutions, the data transmission and latency of GT tasks are compared in Fig. 4. Also, the service- and propulsion-related energy consumptions of different solutions are shown in Fig. 5. These numerical results correspond to the UAV trajectories in Figs. 2 and 3. According to the results shown in the cumulative distribution function (CDF) form in Fig. 5, BL-1 causes the most energy consumption both on service (the energy consumed by MC on executing the task and the UAV–GT links on data transmission) and UAV propulsion. BL-2 leads to the least energy consumption on UAV propulsion. OP consumes fairly less energy than BL-1 and more energy than BL-2 on UAV propulsion. Moreover, OP causes the least energy consumption on service. As shown in Fig. 4, BL-1 leads to the highest data transmission rate via downlinks due to it controls the UAV flying close to GTs. However, the BL-1 does not necessarily

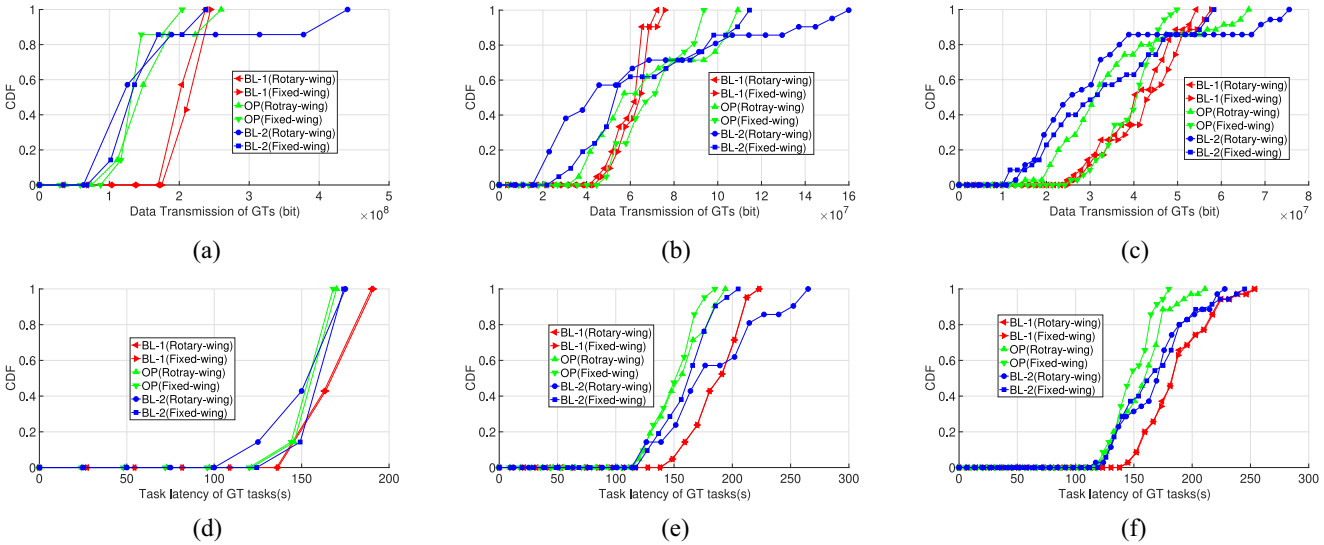

Fig. 4. Data transmission and latency of each GT task led by different solutions. (a) and (d) Spare scenario. (b) and (e) Medium scenario. (c) and (f) Densified scenario.

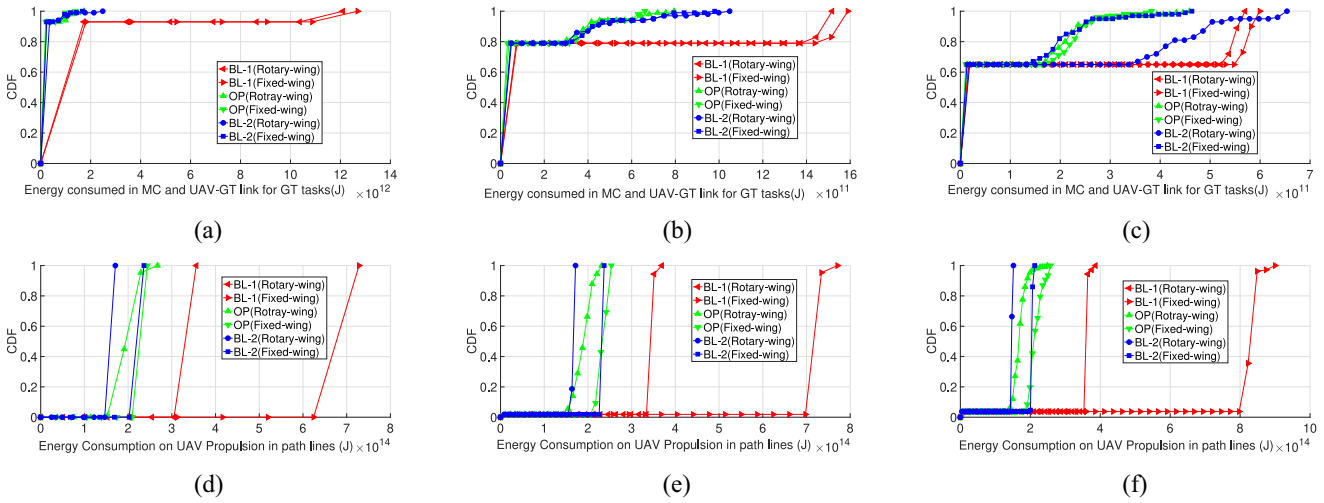

Fig. 5. Energy consumption in MCs and UAV–GT links and on UAV propulsion led by different solutions. (a) and (d) Spare scenario. (b) and (e) Medium scenario. (c) and (f) Densified scenario.

support the shortest latencies of GT tasks in contrast to OP and BL-2. This is because the BL-1 adopts the water-filling-based resource allocation that cannot support the UAV–GT pairs sharing the communication and computation resources efficiently. In contrast, OP and BL-2 support each task finished with the same level of task latency, and OP even leads to the least task latencies in medium and congested GT scenarios. Therefore, we validate that OP works energy efficiently. In addition, we can find in Fig. 5 that the fixed-wing UAV will consume more propulsion energy compared to the rotary-wing UAV in each GT scenario, which follows the real situations. As a result, we can generally conclude that OP has the highest energy efficiency compared to BL-1 and BL-2, with respect to different UAV styles and GT scenarios.

Furthermore, the resource allocation results of different solutions are demonstrated in Fig. 6. As demonstrated, BL-1 adopts the water-filling method to greedily allocate more channels, transmission power, and computation capacities to UAV–GT pairs in contrast to BL-2 and OP. Thus, the service-related energy consumptions led by BL-1 will be higher than BL-2 and OP as shown in Fig. 5. Also, it can be found that BL-2 will allocate more resources to UAV–GT pairs to have a lower resource efficiency compared to OP, especially, in the medium and densified scenarios. This is because, compared to OP, BL-2 only supports weak UAV–GT links to maximally save the propulsion energy. Thus, BL-2 has to allocate more communication and computation resources to the weaker linked UAV–GT pairs to support the UAV finishing GT tasks before their completion deadlines.

In addition, to analyze the performance of the UAV-enabled edge-cloud system against those considered three GT distribution scenarios, we find that each GT could have the highest data transmission rate and lowest latency in the sparse scenario, while they will be the worst in the densified scenario, as shown in Fig. 4. This is due to the GT in the sparse scenario could obtain more communication resource (channels),

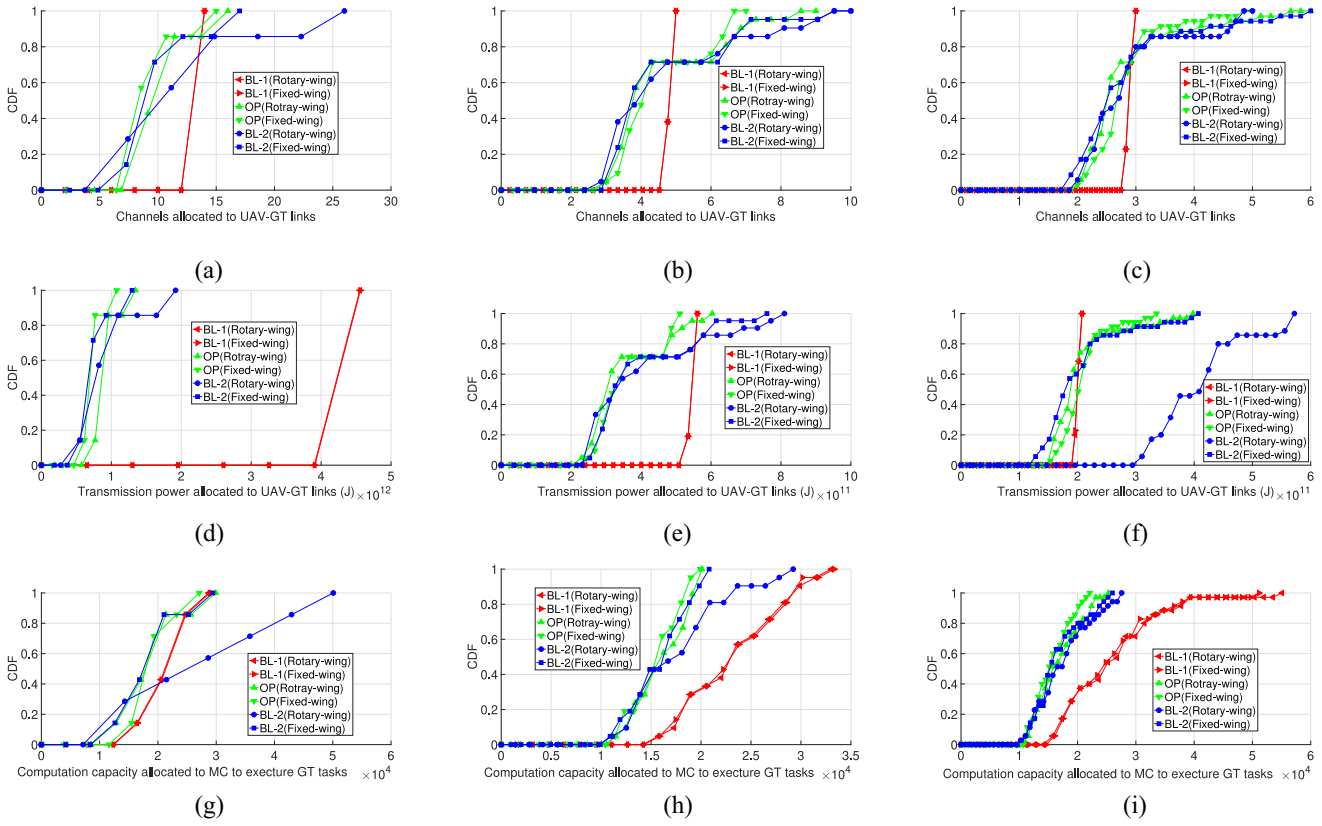

Fig. 6. Resource allocations led by different solutions in the UAV-enabled edge-cloud system. (a), (d), and (g) Spare scenario. (b), (e), and (h) Medium scenario. (c), (f), and (i) Densified scenario.

transmission power, and computation capacity compared to the medium and densified scenarios as shown in Fig. 6. From the perspective of energy consumption, we can find that the GTs in the sparse scenario will consume more service-related energy compared to the ones in the medium and densified scenarios, because they take up more resources as shown in Fig. 5. And the propulsion energy of the UAV will be in the same level among all the GT distribution scenarios. Based on the analysis, we find that the numerical results from simulation follow the real situation.

In conclusion, we validate that OP outperforms BL-1 and BL-2, and can support energy-efficient performance of the UAV-enabled edge-cloud system.

V. Conclusion

In this article, to minimize the energy consumption of UAV in the UAV-enabled edge-cloud system, a suboptimal solution had been proposed to work out the joint trajectory-resource optimization problem by leveraging the SCO and Lagrange duality techniques. The proposed solution had been validated through simulations where a series of comparisons to the baseline solutions have been applied. The numerical results show that the proposed solution indeed leads to a better energy-efficient performance of the UAV-enabled MEC. For future work, we intend to solve the joint trajectory-resource optimization problem of the UAV-enabled MEC using the deep reinforcement learning technique [50], which will support the optimization in an online manner and make the UAV-enabled MEC be more applicable in practical applications. On the other hand, the work in this article only supports the GTs having their basic requests being fulfilled in its MC on the edge and cloud, which leaves more opportunity for the future work to enable UAV-enabled MEC to finish GT tasks with higher QoS. Finally, this article has not studied the cooperation, i.e., interplaying, between the UAV-enabled MEC and central cloud in detail during the task offloading. Thus, we further plan to extend this point to lead to more effective performance of the UAV-enabled edge-cloud system.

References

[1] S. W. Loke. (Jul. 2015). *The Internet of Flying-Things: Opportunities and Challenges With Airborne Fog Computing and Mobile Cloud in the Clouds*. [Online]. Available: https://arxiv.org/pdf/1507.04492.pdf

[2] A. Merwaday and I. Güvenç, "UAV assisted heterogeneous networks for public safety communications," in *Proc. IEEE Wireless Commun. Netw. Conf. (WCNC)*, Mar. 2015, pp. 329–334.

[3] M. Mozaffari, W. Saad, M. Bennis, and M. Debbah, "Mobile Internet of Things: Can UAVs provide an energy-efficient mobile architecture?" in *Proc. IEEE Global Commun. Conf. (GLOBECOM)*, Dec. 2016, pp. 1–6.

[4] Y. Zeng, R. Zhang, and T. J. Lim, "Wireless communications with unmanned aerial vehicles: Opportunities and challenges," *IEEE Commun. Mag.*, vol. 54, no. 5, pp. 36–42, May 2016.

[5] A. Al-Hourani, S. Kandeepan, and S. Lardner, "Optimal LAP altitude for maximum coverage," *IEEE Wireless Commun. Lett.*, vol. 3, no. 6, pp. 569–572, Dec. 2014.

[6] J. Lyu, Y. Zeng, R. Zhang, and T. J. Lim, "Placement optimization of UAV-mounted mobile base stations," *IEEE Commun. Lett.*, vol. 21, no. 3, pp. 604–607, Mar. 2017.

[7] R. I. Bor-Yaliniz, A. El-Keyi, and H. Yanikomeroglu, "Efficient 3-D placement of an aerial base station in next generation cellular networks," in *Proc. IEEE ICC*, May 2016, pp. 1–5.

[8] V. V. Chetlur and H. S. Dhillon, "Downlink coverage analysis for a finite 3-D wireless network of unmanned aerial vehicles," *IEEE Trans. Commun.*, vol. 65, no. 10, pp. 4543–4558, Oct. 2017, doi: 10.1109/TCOMM.2017.2722500.
[9] A. Fotouhi, M. Ding, and M. Hassan, "Dynamic base station repositioning to improve performance of drone small cells," in *Proc. IEEE GLOBECOM*, Dec. 2016, pp. 1–6.
[10] Z. Zhou, Y. Li, J. Zhang, and C. Rizos, "Integrated navigation system for a low-cost quadrotor aerial vehicle in the presence of rotors influences," *J. Surveying Eng.*, vol. 143, no. 1, pp. 1–13, 2017.
[11] C. Zhan and H. La, "Energy minimization in Internet-of-Things system based on rotary-wing UAV," *IEEE Wireless Commun. Lett.*, vol. 8, no. 5, pp. 1341–1344, Oct. 2019, doi: 10.1109/LWC.2019.2916549.
[12] D. Yang, Q. Wu, Y. Zeng, and R. Zhang, "Energy trade-off in ground-to-UAV communication via trajectory design," *IEEE Trans. Veh. Technol.*, vol. 67, no. 7, pp. 6721–6726, Jul. 2018.
[13] Y. Zeng, X. Xu, and R. Zhang, "Trajectory design for completion time minimization in UAV-enabled multicasting," *IEEE Trans. Wireless Commun.*, vol. 17, no. 4, pp. 2233–2246, Apr. 2018.
[14] Y. Zeng, J. Xu, and R. Zhang, "Energy minimization for wireless communication with rotary-wing UAV," *IEEE Trans. Wireless Commun.*, vol. 18, no. 4, pp. 2329–2345, Apr. 2019.
[15] Y. Zeng and R. Zhang, "Energy-efficient UAV communication with trajectory optimization," *IEEE Trans. Wireless Commun.*, vol. 16, no. 6, pp. 3747–3760, Jun. 2017.
[16] Y. Du, K. Wang, K. Yang, and G. Zhang, "Energy efficient resource allocation in UAV based MEC system for IoT devices," in *Proc. IEEE Global Commun. Conf. (GLOBALCOM)*, Dec. 2018, pp. 1–6.
[17] Y. Mao, C. You, J. Zhang, K. Huang, and K. B. Letaief, "A survey on mobile edge computing: The communication perspective," *IEEE Commun. Surveys Tuts.*, vol. 19, no. 4, pp. 2322–2358, 4th Quart., 2017.
[18] *Mobile Edge Computing Introductory Technical White Paper*. Accessed: Sep. 1, 2014. [Online]. Available: http://etsi.org/
[19] T. X. Tran, A. Hajisami, P. Pandey, and D. Pompili, "Collaborative mobile edge computing in 5G networks: New paradigms, scenarios, and challenges," *IEEE Commun. Mag.*, vol. 55, no. 4, pp. 54–61, Apr. 2017.
[20] A. Al-Shuwaili and O. Simeone, "Energy-efficient resource allocation for mobile edge computing-based augmented reality applications," *IEEE Wireless Commun. Lett.*, vol. 6, no. 3, pp. 398–401, Jun. 2017.
[21] K. Zhang *et al.*, "Energy-efficient offloading for mobile edge computing in 5G heterogeneous networks," *IEEE Access*, vol. 4, pp. 5896–5907, 2016.
[22] K. Wang, K. Yang, and C. Magurawalage, "Joint energy minimization and resource allocation in C-RAN with mobile cloud," *IEEE Trans. Cloud Comput.*, vol. 6, no. 3, pp. 760–770, Jul./Sep. 2018.
[23] H. Mei, K. Wang, and K. Yang, "Multi-layer cloud-RAN with cooperative resource allocations for low-latency computing and communication services," *IEEE Access*, vol. 5, pp. 19023–19032, 2017.
[24] N. H. Motlagh, M. Bagaa, and T. Taleb, "UAV-based IoT platform: A crowd surveillance use case," *IEEE Commun. Mag.*, vol. 55, no. 2, pp. 128–134, Feb. 2017.
[25] S. Jeong, O. Simeone, and J. Kang, "Mobile cloud computing with a UAV-mounted cloudlet: Optimal bit allocation for communication and computation," *IET Commun.*, vol. 11, no. 7, pp. 969–974, Nov. 2017.
[26] X. Cao, J. Xu, and R. Zhang. (Mar. 2018). *Mobile Edge Computing for Cellular Connected UAV Computation Offloading and Trajectory Optimization*. [Online]. Available: https://arxiv.org/pdf/1803.03733v1.pdf
[27] Q. Hu, Y. Cai, G. Yu, Z. Qin, M. Zhao, and G. Y. Li, "Joint offloading and trajectory design for UAV-enabled mobile edge computing systems," *IEEE Internet Things J.*, vol. 6, no. 2, pp. 1879–1892, Apr. 2019.
[28] J. Xiong, H. Guo, and J. Liu, "Task offloading in UAV-aided edge computing: Bit allocation and trajectory optimization," *IEEE Commun. Lett.*, vol. 23, no. 3, pp. 538–541, Mar. 2019.
[29] M. Hua, Y. Wang, C. Li, Y. Huang, and L. Yang, "UAV-aided mobile edge computing systems with one by one access scheme," *IEEE Trans. Green Commun. Netw.*, vol. 3, no. 3, pp. 664–678, Sep. 2019, doi: 10.1109/TGCN.2019.2910590.
[30] Y. Qian, F. Wang, J. Li, L. Shi, K. Cai, and F. Shu, "User association and path planning for UAV-aided mobile edge computing with energy restriction," *IEEE Wireless Commun. Lett.*, vol. 8, no. 5, pp. 1312–1315, Oct. 2019, doi: 10.1109/LWC.2019.2913843.
[31] S. Zhang, Y. Zeng, and R. Zhang, "Cellular-enabled UAV communication: Trajectory optimization under connectivity constraint," in *Proc. IEEE Int. Conf. Commun. (ICC)*, Kansas City, MO, USA, 2018, pp. 1–6.
[32] J. Pearl, *Heuristics: Intelligent Search Strategies for Computer Problem Solving*. New York, NY, USA: Addison-Wesley, 1983.
[33] M. J. Osborne, *An Introduction to Game Theory*. London, U.K.: Oxford Univ. Press, 2003.
[34] H. Mei, J. Bigham, P. Jiang, and E. Bodanese, "Distributed dynamic frequency allocation in fractional frequency reused relay based cellular networks," *IEEE Trans. Commun.*, vol. 61, no. 4, pp. 1327–1336, Apr. 2013.
[35] I. A. Shah, S. Jan, I. Khan, and S. Qamar, "An overview of game theory and its applications in communication networks," *Int. J. Multidiscipl. Sci. Eng.*, vol. 3, no. 4, pp. 5–11, Apr. 2012.
[36] H. Mei, K. Wang, and K. Yang, "Joint cache content placement and task offloading in C-RAN enabled by multi-Layer MEC," *Sensors*, vol. 18, no. 6, p. 1826, 2018.
[37] S. Boyd and L. Vandenberghe, *Convex Optimization*. Cambridge, U.K.: Cambridge Univ. Press, 2004.
[38] S. Mehrotra, "On the implementation of a primal–dual interior point method," *SIAM J. Optim.*, vol. 2, no. 4, p. 575, 1992.
[39] S. Boyd, "Subgradient method," Stanford Univ., Stanford, CA, USA, 2014. [Online]. Available: https://stanford.edu/class/ee364b/lectures/subgradient_method_notes.pdf
[40] M. Grant and S. Boyd. (2016). *CVX: MATLAB Software for Disciplined Convex Programming*. [Online]. Available: http://cvxr.com/cvx
[41] Z. Yang and X. Liu, "Dynamic clone sharing scheme in mobile cloud computing: A delaunay triangulation approach," in *Proc. IEEE 17th Int. Conf. Comput. Sci. Eng.*, Chengdu, China, 2014, pp. 1320–1325.
[42] Y. Wen, W. Zhang, and H. Luo, "Energy-optimal mobile application execution: Taming resource-poor mobile devices with cloud clones," in *Proc. IEEE INFOCOM*, Orlando, FL, USA, 2012, pp. 2716–2720.
[43] M. Chen, M. Mozaffari, W. Saad, C. Yin, M. Debbah, and C. S. Hong, "Caching in the sky: Proactive deployment of cache-enabled unmanned aerial vehicles for optimized quality-of-experience," *IEEE J. Sel. Areas Commun.*, vol. 35, no. 5, pp. 1046–1061, May 2017.
[44] C. You and R. Zhang, "3D trajectory optimization in Rician fading for UAV-enabled data harvesting," *IEEE Trans. Wireless Commun.*, vol. 18, no. 6, pp. 3192–3207, Jun. 2019.
[45] Y. Guo, S. Yin, and J. Hao, "Resource allocation and 3-D trajectory design in wireless networks assisted by rechargeable UAV," *IEEE Wireless Commun. Lett.*, vol. 8, no. 3, pp. 781–784, Jun. 2019, doi: 10.1109/LWC.2019.2892721.
[46] Q. Wu and R. Zhang, "Common throughput maximization in UAV-enabled OFDMA systems with delay consideration," *IEEE Trans. Commun.*, vol. 66, no. 12, pp. 6614–6627, Dec. 2018.
[47] J. Chen, F. Ye, and Y. Li, "Travelling salesman problem for UAV path planning with two parallel optimization algorithms," in *Proc. Progr. Electromagn. Res. Symp. Fall (PIERS-FALL)*, Singapore, 2017, pp. 832–837.
[48] A. Ben-Tal and A. Nemirovski, *Lectures on Modern Convex Optimization: Analysis, Algorithms, and Engineering Applications*, vol. 2. Philadelphia, PA, USA: SIAM, 2001.
[49] J. Jang and K. B. Lee, "Transmit power adaptation for multiuser OFDM systems," *IEEE J. Sel. Areas Commun.*, vol. 21, no. 2, pp. 171–178, Feb. 2003.
[50] H. Van Hasselt, A. Guez, and D. Silver, "Deep reinforcement learning with double *Q*-learning," in *Proc. AAAI*, 2016, pp. 2094–2100.

Haibo Mei received the B.Sc. and M.Sc. degrees from the School of Computer Science and Engineering, University of Electronic Science and Technology of China, Chengdu, China, in 2005 and 2008, respectively, and the Ph.D. degree from the School of Electronic Engineering and Computer Science, Queen Mary University of London (QMUL), London, U.K. in 2012.

He was a Postdoctoral Research Assistant with QMUL and a Senior Research and Development Engineer with Securus Software, Ltd, Leatherhead, U.K. He is currently a Lecturer with the School of Aeronautics and Astronautics, and a Postdoctoral Fellow with the School of Communication and Information Engineering, University of Electronic Science and Technology of China. His research interests include resource efficiency and self-organization of wireless communications, intelligent transportation system, and mobile cloud computing.

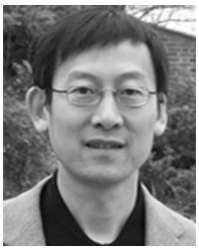

Kun Yang (SM'08) received the M.Sc. and B.Sc. degrees from the Computer Science Department, Jilin University, Changchun, China, and the Ph.D. degree from the Department of Electronic and Electrical Engineering, University College London, London, U.K.

He is currently a Chair Professor with the School of Computer Science and Electronic Engineering, University of Essex, Colchester, U.K., leading the Network Convergence Laboratory, U.K. He is also an Affiliated Professor with the University of Electronic Science and Technology of China, Chengdu, China. His main research interests include wireless networks, network convergence, future Internet technology, data and energy cooperation, and mobile computing. He manages research projects funded by various sources, such as U.K. EPSRC, EU FP7/H2020, and industries. He has published over 200 papers.

Dr. Yang serves on the editorial boards of both IEEE and non-IEEE journals.

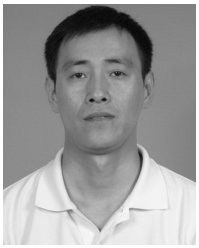

Qiang Liu (M'14) received the B.Sc., M.Sc., and Ph.D. degrees from the School of Information and Communication, University of Electronic Science and Technology of China, Chengdu, China, in 1996, 2000, and 2012, respectively.

He is currently an Associate Professor with the University of Electronic Science and Technology of China. His main research interests include wireless communication networks, Internet of Things, low power WAN, and molecular communication.

Dr. Liu has been a member of IEEE ComSoc.

Kezhi Wang (M'15) received the B.E. and M.E. degrees from the College of Automation, Chongqing University, Chongqing, China, in 2008 and 2011, respectively, and the Ph.D. degree from the University of Warwick, Coventry, U.K., in 2015.

He was a Senior Research Officer with the University of Essex, Colchester, U.K. He is currently a Lecturer with the Department of Computer and Information Sciences, Northumbria University, Newcastle upon Tyne, U.K. His research interests include wireless communication, signal processing, and mobile cloud computing.